Earth-Science Reviews 203 (2020) 103137

Contents lists available at ScienceDirect

Earth-Science Reviews

journal homepage: www.elsevier.com/locate/earscirev

Sequence stratigraphy in organic-rich marine mudstone successions using chemostratigraphic datasets

Maya T. LaGrange*, Kurt O. Konhauser, Octavian Catuneanu, Brette S. Harris, Tiffany L. Playter, Murray K. Gingras

Department of Earth and Atmospheric Sciences, University of Alberta, 1-26 Earth Sciences Building, Edmonton, AB T6G 2E3, Canada

ARTICLE INFO

Keywords:
Sequence stratigraphy
Chemostratigraphy
Organic-rich mudstone
Black shale
Geochemical proxies

ABSTRACT

Sequence stratigraphy is commonly used to understand basin history and the distribution of conventional reservoir facies. Establishing a sequence stratigraphic framework in organic-rich mudstone successions is challenging because macroscale sedimentological and petrophysical variations can be subtle, while biostratigraphic and seismic data may be unavailable or of limited use. For these reasons, it is becoming increasingly common for chemostratigraphic profiles to be integrated with other datasets to facilitate sequence stratigraphic interpretation. This paper summarizes the whole-rock inorganic geochemical proxies relevant to sequence stratigraphic analysis in fine-grained, organic-rich marine units and reviews studies that have incorporated chemostratigraphic trends for sequence stratigraphy. This synthesis demonstrates that chemostratigraphic datasets are useful in identification of transgressive-regressive cycles, allowing for a preliminary summary of the chemostratigraphic characteristics of the maximum flooding surface, maximum regressive surface, transgressive systems tract, and regressive systems tract to be established based on existing work. A preliminary synthesis of the chemostratigraphic characteristics of the highstand systems tract is also possible for highstand systems tracts recognized using other criteria. However, a chemostratigraphic means of identifying the correlative conformity and basal surface of forced regression in order to subdivide the regressive systems tract into the lowstand systems tract, falling-stage systems tract, and highstand systems has not yet been demonstrated. Further work is also required in order to establish the differences in the chemostratigraphic signature of surfaces and systems tract depending on the depositional setting. Chemostratigraphic proxies are an emergent and promising tool for the identification of cyclicity in organic-rich mudstone intervals, which will become increasingly useful as further research is conducted on the topic.

1. Introduction

Sequence stratigraphy was defined by Posamentier and Allen (1999) as "the analysis of cyclic sedimentation patterns that are present in stratigraphic successions, as they develop in response to variations in sediment supply and space available for sediment to accumulate" (p.1). In sequence stratigraphy, the unit deposited during one of these complete cycles is classified as a sequence (Catuneanu et al., 2009), and sequences are subdivided into systems tracts that consist of coeval depositional systems (Brown Jr. and Fisher, 1977). Systems tracts can be further subdivided into smaller scale sequence stratigraphic cycles (i.e., sequences), allostratigraphic cycles (i.e., parasequences), or sedimentological cycles (i.e., beds and bedsets) (Catuneanu, 2019a). Both sequences and systems tracts are bounded by sequence stratigraphic surfaces (Embry, 2002; Catuneanu, 2006; Catuneanu et al., 2009). Sequence stratigraphic units and bounding surfaces can be observed at different scales (i.e., hierarchical levels), depending on the purpose of study and/or the resolution of the data available (Catuneanu, 2019b).

The interpretations drawn from sequence stratigraphic analysis are used to gain insights into the evolution of sedimentary basins and predict facies distributions for hydrocarbon and mineral exploration (Embry, 2009; Catuneanu et al., 2011). Recently, the development of shale resource plays has resulted in an increased focus on understanding and predicting lateral and vertical lithological variations in organic-rich mudstone successions (e.g., Egenhoff and Fishman, 2013; Taylor and Macquaker, 2014; Wilson and Schieber, 2015; Birgenheier et al., 2017; Li and Schieber, 2020). As a result, establishing a sequence stratigraphic framework is a valuable tool for the evaluation of these successions because it allows for the delineation and subsurface correlation of higher quality reservoir intervals (Slatt and Rodriguez, 2012;

* Corresponding author.
E-mail address: maya1@ualberta.ca (M.T. LaGrange).

https://doi.org/10.1016/j.earscirev.2020.103137
Received 4 July 2019; Received in revised form 13 February 2020; Accepted 14 February 2020
Available online 19 February 2020
0012-8252/

Knapp et al., 2019).

However, making stratigraphic correlations in mudstone intervals presents unique challenges. These successions are characterized by more subtle macroscale sedimentological variations than those observed in coarser-grained clastic and carbonate successions, making lithological trends less feasible unless thin sections are available at a high resolution (Ratcliffe et al., 2012a; Borcovsky et al., 2017). Furthermore, the subtle compositional variability characteristic of fine-grained successions can be difficult to infer from petrophysical datasets (i.e., well logs), which are commonly used as a basis for stratigraphic correlations (Pearce et al., 2005; Turner et al., 2016; Knapp et al., 2019). In addition, as these mudstone intervals commonly represent sedimentation in distal areas of restricted basins, biostratigraphic datasets may be unavailable or of limited use (Ratcliffe et al., 2012a). Moreover, high-resolution biostratigraphic datasets are typically unavailable for Paleozoic or older mudstone intervals (Slatt and Rodriguez, 2012). The stratal geometries that allow researchers to make interpretations using seismic profiles are often absent (Pearce et al., 2005), seismic datasets may not exist, or the scale of the sequence stratigraphic analysis may be sub-seismic (Catuneanu, 2019b).

Given these challenges, it is becoming increasingly common for chemostratigraphic data to be integrated with other datasets in the study of mudstone successions (e.g., Pearce et al., 1999; Ratcliffe et al., 2010, 2012a, 2012b; Sano et al., 2013; Turner et al., 2015, 2016; El Attar and Pranter, 2016; Nyhuis et al., 2016; Pyle and Gal, 2016; Playter et al., 2018; DeReuil and Birgenheier, 2019). This type of stratigraphy uses inorganic geochemical properties of whole-rock samples to characterize and correlate stratigraphic units (Pearce et al., 1999). More specifically, certain elements and elemental ratios are used as proxies for sediment provenance, paleoproductivity, paleoredox conditions in the water column and/or sediment pile, and other environmental conditions at the time of sediment deposition. Indeed, observed variations in these proxies with depth have been used to identify chemostratigraphic units with distinct geochemical characteristics (Pearce et al., 1999). As a result, chemostratigraphic units are now frequently applied as a means of subdivision and correlation (e.g., Pearce et al., 1999; Ratcliffe et al., 2010, 2012a; El Attar and Pranter, 2016; Pyle and Gal, 2016). Chemostratigraphic datasets have also been used to increase the resolution of sequence stratigraphic interpretations within mudstone intervals (e.g., Algeo et al., 2004; Ver Straeten et al., 2011; Hammes and Frébourg, 2012; Sano et al., 2013; Turner et al., 2015, 2016).

In this work, we review the elements and elemental ratios that can be used as chemostratigraphic proxies for sequence stratigraphic interpretation of organic-rich mudstone successions. Through this review, we aim to provide a systematic framework for the chemostratigraphic identification of sequence stratigraphic surfaces, systems tracts, and sequences in organic-rich mudstone intervals. This work follows the sequence stratigraphic terminology of Catuneanu (2019a) (Fig. 1). Herein, 'mudstone' is used as a general term referring to all fine-grained sedimentary rocks and is defined as a rock composed of greater than 50% silt and clay size grains following Lazar et al. (2015).

2. Chemostratigraphic proxies

The following section reviews many of the elemental proxies useful to chemostratigraphy of mudstone intervals and how they are interpreted. Table 1 summarizes the main mineralogical controls on these elements, although there are other ways for these elements to become enriched in sediment (e.g., incorporation into nodules; adsorption onto mineral particles in the water column; adsorption onto, or accumulation into, organic matter; diagenetic and metamorphic reactions, and interactions with secondary fluids). To confirm the primary controls on each element, many studies compare elemental composition data to mineralogical data obtained through x-ray diffraction analysis and perform statistical analyses such as Principal Component Analysis,

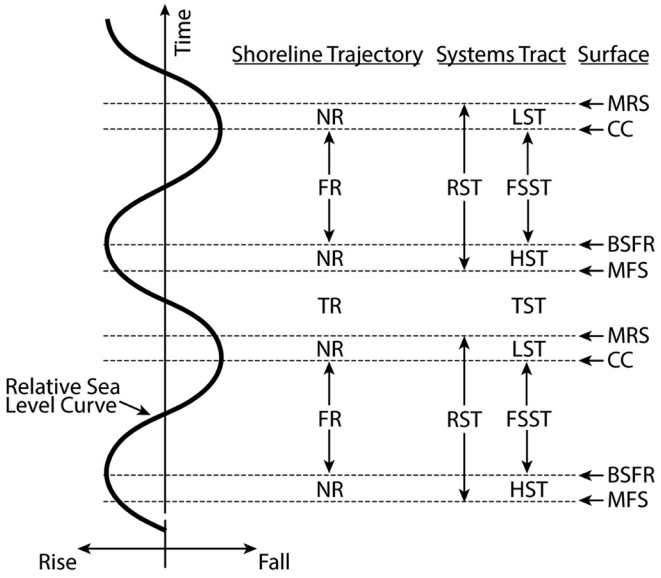

Fig. 1. Sequence stratigraphic terminology used herein. Acronyms: NR–normal regression; FR–forced regression; TR–transgression; RST–regressive systems tract; LST–lowstand systems tract; FSST–falling-stage systems tract; HST–highstand systems tract; TST–transgressive systems tract; MRS–maximum regressive surface; CC–correlative conformity; BSFR–basal surface of forced regression; and MFS–maximum flooding surface. Modified from Catuneanu (2006).

Hierarchical Cluster Analysis, or Q-mode Factor Analysis to determine elemental associations (e.g., Pearce et al., 2005; Ver Straeten et al., 2011; Ratcliffe et al., 2012a; Sano et al., 2013; Turner et al., 2016; Playter et al., 2018). Table 2 summarizes the purpose of each elemental proxy discussed below. It is critical that elemental data are tied to mineralogical-data calibration points to ensure sound and accurate depositional and diagenetic interpretations of elemental data as they relate to mineralogical distribution.

2.1. Detrital sediment

The abundance of elements that are predominantly associated with detrital sediment can be used to make inferences about the abundance of terrigenous (i.e., continental) sediment input into the basin (Chen et al., 2013). These elements will vary depending on the interval but commonly include Al, K, Ti, and Zr (e.g., Pearce et al., 2005; Ratcliffe et al., 2012b; Sano et al., 2013; Nyhuis et al., 2016; Turner et al., 2016). In addition to single element patterns, summing a combination of the elements has also proven effective as a proxy for abundance of continental input (e.g., Al_2O_3 + TiO_2 + Fe_2O_3 + K_2O) as was used by Ratcliffe et al. (2012b) to characterize chemostratigraphic units in the Horn River Formation (British Columbia, Canada). Similarly, Sano et al. (2013) used Al_2O_3 + K_2O + TiO_2 in conjunction with other proxies to establish a chronostratigraphic framework in the Haynesville Formation (Texas and Louisiana). Chen et al. (2013) suggested that because Ti is present in heavier minerals (e.g., rutile, ilmenite) that settle out sooner than Al bearing minerals, the molar Ti/Al ratio can be used as a proxy for changes in proximity to detrital sediment sources and variation in relative sea level in intervals where sediment provenance remains constant. They observed similar trends in the reconstructed sea level profile based on benthic $\delta^{18}O$ profile and the Ti/Al profile of sediment cores from the South China Sea and Japan Sea, with lower Ti/Al in sediment deposited during interglacial periods and higher Ti/Al in sediments from glacial periods suggesting that increases in Ti/Al reflect increased continental sediment supply to the basin.

Table 1
Primary mineralogical controls on elements commonly used as chemostratigraphic proxies in organic-rich mudstone successions.

Element	Typical mineralogical affinity	Reference
Al	Clay and feldspar.	Ratcliffe et al. (2004), Brumsack (2006), Tribovillard et al. (2006), Piper and Calvert (2009)
Cr	Chromite, clay minerals, ferromagnesian minerals.	Tribovillard et al. (2006)
K	Clay and feldspar.	Ratcliffe et al. (2004), Turner et al. (2016)
Nb	Titanium oxides, silicates, or distinct mineral phase, clay minerals.	Bonjour and Dabard (1991), Dinelli et al. (2007)
Rb	Clay and feldspar.	Ratcliffe et al. (2004), Dinelli et al. (2007)
Th	Detrital. Associated with clay minerals, accessory minerals or adsorbed to mineral surfaces.	Myers and Wignall (1987), Rowe et al. (2017)
Ti	Titanium oxides, chlorite, illite/mica, biotite.	Ratcliffe et al. (2004), Pearce et al. (2005), El Attar and Pranter (2016)
U	Detrital or authigenic. Accessory minerals or adsorbed to mineral surfaces. Can also be adsorbed to organic matter or precipitated as uranium oxides.	Myers and Wignall (1987), Wignall and Twitchett (1996), Tribovillard et al. (2006)
Y	Heavy minerals (zircon, garnet, monzanite, apatite, hornblende).	Dinelli et al. (2007)
Zr	Zircon.	Patchett et al. (1984), Ratcliffe et al. (2004), Mongelli et al. (2006), El Attar and Pranter (2016)

Table 2
Elemental proxies useful for interpreting systems tracts, bounding surfaces, and sequences in marine organic-rich mudstone successions.

Parameter	Potential proxies	Details	Reference
Detrital Sediment	Elements predominantly associated with detrital sediment	Vary depending on the interval but commonly include Al, K, Zr, and Ti.	e.g., Pearce et al. (2005), Ratcliffe et al. (2012b), Sano et al. (2013), Nyhuis et al. (2016), Turner et al. (2016)
	Sums of detrital elements	For example, $Al_2O_3 + TiO_2 + Fe_2O_3 + K_2O$ used by Ratcliffe et al. (2012b) or $Al_2O3 + K_2O + TiO_2$ used by Sano et al. (2013).	e.g., Ratcliffe et al. (2012b), Sano et al. (2013)
	Ti/Al	Higher Ti/Al as terrigenous input increases.	Chen et al. (2013)
Grain Size	Si/Al	If silica is primarily detrital, can reflect changes in abundance of coarse sediment supply.	e.g., Ratcliffe et al. (2004), Dinelli et al. (2007), Ratcliffe et al. (2012c)
	Zr/Al	May reflect changes in abundance of coarse sediment supply.	e.g., Ratcliffe et al. (2004), Dinelli et al. (2007)
	Zr/Nb	May reflect changes in abundance of coarse sediment supply.	e.g., Ratcliffe et al. (2006), Sano et al. (2013)
	Zr/Rb	May reflect changes in abundance of coarse sediment supply.	e.g., Dinelli et al. (2007)
	Y/Al	Reflects changes in abundance of coarse sediment supply.	e.g., Dinelli et al. (2007)
	Y/Rb	May reflect changes in abundance of coarse sediment supply.	e.g., Dinelli et al. (2007)
Paleoredox	V	Can become enriched in anoxic to euxinic environments.	Wanty and Goldhaber (1992), Calvert and Pedersen (1993), Tribovillard et al. (2006)
	Re	Can become enriched in anoxic to euxinic environments.	Colodner et al. (1993), Crusius et al. (1996), Yamashita et al. (2007)
	Cr	Can become enriched in anoxic to euxinic environments.	Calvert and Pedersen (1993), Algeo and Maynard (2004), Tribovillard et al. (2006)
	U	Can become enriched in anoxic to euxinic environments.	Myers & Wignall (1987), Wignall and Twitchett (1996), McManus et al. (2005), Tribovillard et al. (2006)
	Mo	Can become enriched in euxinic environments.	Erickson and Helz (2000)
	Ni	Can become enriched in euxinic environments	Huerta-Diaz and Morse (1992), Calvert and Pedersen (1993), Tribovillard et al. (2006)
	Th/U	Th/U $<$ 2 reflects anoxic conditions, Th/U 2–7 suggests oxic environments, and Th/U $>$ 7 is indicative of sediment deposited under highly oxidizing conditions.	Wignall and Twitchett (1996)
Basin Restriction	Mo/TOC	Mo/TOC $> 35 \times 10^{-4}$ in weakly restricted settings, ~15–35 $\times 10^{-4}$ in environments characterized by moderate restriction, and $< 15 \times 10^{-4}$ in strongly restricted settings.	Algeo & Lyons (2006)
Excess Silica	Peaks in Si/Al	Al typically reflects clay abundance in mudstones (Sageman and Lyons, 2004; Rowe et al., 2017).	Davis et al. (1999), Sageman & Lyons (2004), Turner et al. (2015, 2016), Gambacorta et al. (2016), Zhang et al. (2019)
	Si-Al crossplot	See Fig. 2.	Tribovillard et al. (2006), Rowe et al. (2012), El Attar and Pranter (2016)
	$Si_{excess} = Si_{sample}(Si/Al)_{average\ shale}$	Excess silica relative to average shale.	Ross and Bustin (2009), Shen et al. (2014), Arsairai et al. (2016)

Acronyms: TOC–total organic carbon.

2.2. Grain size

Chemostratigraphic proxies can also be used to infer grain size variations. For instance, if the Si present in an interval is predominantly detrital, trends in Si/Al can reflect variations in the proportion of silt to clay size fraction (e.g., Ratcliffe et al., 2004; Dinelli et al., 2007; Ratcliffe et al., 2012c). Similarly, changes in Zr/Nb and Zr/Al can indicate changes in the abundance of coarse sediment supply if these ratios are primarily controlled by variations in the abundance of silt-size detrital zircon rather than variations in provenance (Ratcliffe et al.,

2004, 2006; Dinelli et al., 2007; Sano et al., 2013). In this case, Ratcliffe et al. (2004) suggested that increasing Zr/Al results from an increased proportion of silt-size detrital zircon compared to clay minerals, whereas Ratcliffe et al. (2006) and Sano et al. (2013) observed that Zr/Nb followed grain size trends with higher Zr/Nb in coarser grained intervals. Additionally, in a study of fine-grained Pleistocene and Holocene sediments, Dinelli et al. (2007) showed that ratios of Zr/Rb, Zr/Al, Y/Al, and Y/Rb correlated well to the coarse silt-size sediment fraction. Bloemsma et al. (2012) assessed geochemical grain size proxies for three offshore fine-grained quaternary sediment cores. Two of these cores were retrieved from different locations off the coast of West Africa, whereas the third core was collected off the coast of Chile. In the two cores from West Africa, Si exhibited the strongest correlations with mean grain size, whereas Ti showed the strongest correlations with mean grain size for core collected offshore of Chile. Based on these results, Bloemsma et al. (2012) concluded that geochemical grain size proxies vary depending on the particular setting. The above studies suggest that geochemical grain size proxies should be determined for each interval on a case by case basis through comparison with grain size data.

2.3. Paleoredox

Variations in redox conditions changes the solubility of many elements, with decreased oxygen levels at the sediment water interface resulting in the enrichment of certain metals in sediment; in this paper we focus on mudstone successions. When discussing paleoredox conditions, the terms oxic, suboxic, anoxic, and euxinic are used. The distinction between oxic, suboxic, and anoxic has commonly been used to distinguish the amount of dissolved oxygen available, with different authors using different concentrations (e.g., oxic, > 4.5 uM; suboxic, 4.5 uM – 10 nM; anoxic, < 10 nM; Morrison et al., 1999; Revsbech et al., 2009; Tyson and Pearson, 1991). The terms are similarly used to refer to specific microbial metabolisms and the terminal electron acceptor (TEA) coupled to the oxidation of organic carbon (e.g., Froelich et al., 1979; Canfield and Thamdrup, 2009). Thus, oxic refers to aerobic respiration (where cells use O_2), suboxic refers to using nitrate (NO_3^-), while anoxic refers to using Mn(IV), Fe(III) or sulfate (SO_4^{2-}) (Konhauser, 2007). Additionally, the term euxinic will be used herein to describe anoxic conditions in which sulfate reduction results in the presence of hydrogen sulfide in the water column.

Trace element enrichment is commonly compared to an average shale with the enrichment factor for a given element (X) calculated as follows (Brumsack, 2006; Tribovillard et al., 2006):

$$EF_X = (X/Al)_{sample}/(X/Al)_{average\ shale} \quad (1)$$

An element is considered to be enriched if this ratio exceeds 1 and depleted if the ratio is below 1 (Brumsack, 2006; Tribovillard et al., 2006). Alternatively, Brumsack (2006) argued that for intervals with low detrital input and, therefore low Al abundance, it is more suitable to evaluate enrichment of an element (X) by considering its non-detrital fraction, which can be calculated using the following formula:

$$X_{non-detrital} = X_{sample} - Al_{sample}\,(X/Al)_{average\ shale} \quad (2)$$

Elemental concentrations from Average Shale (Wedepohl, 1971) or Post-Archean Average Australian Shale (Taylor and McLennan, 1985) are commonly used as comparators (e.g., Ross and Bustin, 2009; Rowe et al., 2009; Zhou and Jiang, 2009; Gambacorta et al., 2016).

Several trace elements, including V, Re, Cr, and U, may become enriched in anoxic to euxinic sediment. Vanadium is fixed in sediment under mildly anoxic conditions if the insoluble hydroxide $VO(OH)_2$ is formed once V(V) is reduced to V(IV) (Wanty and Goldhaber, 1992; Calvert and Pedersen, 1993). Under euxinic conditions, sedimentary V enrichment occurs through precipitation of V_2O_3 or $V(OH)_3$ upon reduction of V(IV) to V(III) (Wanty and Goldhaber, 1992; Calvert and Pedersen, 1993). Sedimentary enrichment of Re occurs under anoxic to euxinic conditions where Re(VII) is reduced to Re(IV) (Colodner et al., 1993; Crusius et al., 1996; Yamashita et al., 2007) and precipitated as sulfides or adsorbed to organic matter (Kendall et al., 2010). In anoxic settings, the conversion of Cr(VI) to Cr(III) leads to the latter being incorporated into organic compounds or Fe(III) and Mn(IV) oxyhydroxides (Calvert and Pedersen, 1993; Algeo and Maynard, 2004). Chromium has been used to interpret paleoredox conditions in some studies (e.g., El Attar and Pranter, 2016), although the possibility of Cr loss from remineralization of organic matter in euxinic conditions (Algeo and Maynard, 2004) and the potential for Cr enrichment from an increased proportion of Cr in detrital sediment means that this proxy should be used with caution (Tribovillard et al., 2006).

Uranium is delivered to the oceans in detrital accessory minerals and in solution in the form of U(VI) (Myers and Wignall, 1987). Under oxic conditions, U(VI) binds with bicarbonate to form a soluble anion, while reducing conditions lead to the conversion of U(VI) to U(IV) and can lead to sedimentary enrichment of U in the form of uraninite, UO_2 (Myers and Wignall, 1987; Klinkhammer and Palmer, 1991; Wignall and Twitchett, 1996; McManus et al., 2005; Partin et al., 2013).

Molybdenum accumulates in sediment under euxinic conditions (Helz et al., 1996; Tribovillard et al., 2006; Scott and Lyons, 2012; Robbins et al., 2016). In seawater, Mo is present as molybdate (MoO_4^{2-}) and in the presence of H_2S reacts to form particle-reactive thiomolybdates (e.g., MoS_4^{2-}) (Helz et al., 1996), which is enriched in sediment through complexation with organic matter or reduced compounds (Helz et al., 1996; Erickson and Helz, 2000). Similarly, euxinic conditions result in enrichment of Ni through incorporation of NiS into sulfides (Huerta-Diaz and Morse, 1992; Calvert and Pedersen, 1993).

The Th/U ratio can be used as an indicator of paleoredox conditions (Myers and Wignall, 1987; Wignall and Twitchett, 1996; Kimura and Watanabe, 2001; Sano et al., 2013). As previously discussed, U can become enriched in sediment under anoxic conditions (Myers and Wignall, 1987; Wignall and Twitchett, 1996; Partin et al., 2013). In contrast, the abundance of Th in sediment is controlled by detrital input as it is insoluble in seawater, and consequently it does not become authigenically enriched (Myers and Wignall, 1987; Wignall and Twitchett, 1996). Owing to their differing mobility, Th/U < 2 is interpreted to reflect deposition under anoxic conditions, Th/U of 2–7 suggests oxic environments, and Th/U > 7 are indicative of sediment deposited under highly oxidizing conditions (Wignall and Twitchett, 1996).

2.4. Basin restriction

In basins characterized by a degree of restriction from the global oceans, Algeo & Lyons (2006) proposed that Mo/total organic carbon (TOC) is an indicator of the extent of basin isolation. In that study, Mo–TOC relationships of sediment were demonstrated to vary as a function of deep-water dissolved Mo and deep-water renewal time in several restricted modern anoxic environments. Algeo & Lyons (2006) observed sedimentary Mo/TOC values of $> 35 \times 10^{-4}$ in weakly restricted settings, ~15–35 $\times 10^{-4}$ in environments characterized by moderate restriction, and $< 15 \times 10^{-4}$ in strongly restricted settings. This trend was interpreted to reflect a growing drawdown of the aqueous Mo reservoir in increasingly restricted settings caused by Mo removal to sediment outpacing Mo re-supply. These relationships have been used to interpret the level of basin isolation in several studies of organic-rich mudstone intervals including Harris et al. (2013), Turner and Slatt (2016), and Hines et al. (2019).

2.5. Biogenic sediment

Certain elements, elemental ratios, and cross-plots are used to estimate the proportion of biogenic silica (i.e., silica derived from organisms such as diatoms, radiolarians, or siliceous sponges) relative to other sources of silica. Understanding variations in the abundance of

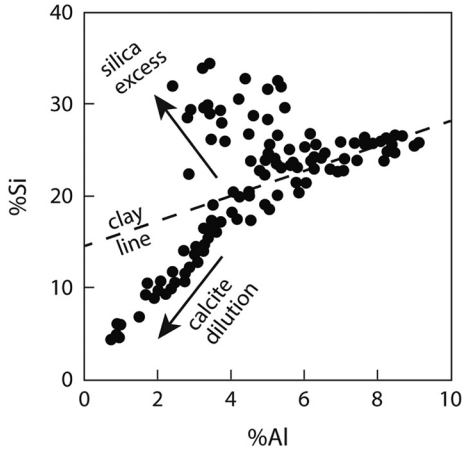

Fig. 2. Example of a Si–Al cross-plot used to identify excess silica. Data is from the Barnett Shale in the 1-Blakely core in Wise County, Texas. Reproduced from Rowe et al. (2012) with permission.

biogenic silica is important because these trends can be used to interpret variations in productivity (Schieber et al., 2000; Harris et al., 2018) or variations in the degree of clastic dilution, with higher biogenic silica suggestive of condensed deposition (Bohacs, 1998; Gutierrez Parades et al., 2017). Sources of Si in mudstone successions include detrital Si from fluvial or aeolian sources, precipitation of silica during clay diagenesis, and biogenic silica (Schieber, 1996; Taylor & Macquaker, 2014). Hydrothermal input can additionally serve as a potential source of silica in mudstone intervals (e.g., Adachi et al., 1986; Arsairai et al., 2016). Aluminium content typically reflects clay abundance in mudstone intervals (Sageman and Lyons, 2004; Rowe et al., 2017). Excess Si relative to Al is typically identified in the following three ways: (1) peaks in Si/Al (e.g. Dean and Arthur, 1998; Davis et al., 1999; Sageman and Lyons, 2004; Turner et al., 2016); (2) Si–Al crossplots (Fig. 2; Tribovillard et al., 2006; Rowe et al., 2012; El Attar and Pranter, 2016); and (3) calculating excess silica relative to the average shale using eq. 3 (e.g., Ross and Bustin, 2009; Shen et al., 2014; Arsairai et al., 2016). Where excess Si may be biogenic, aeolian, or hydrothermal in origin.

$$Si_{excess} = Si_{sample} - Al_{sample}\,(Si/Al)_{average\ shale} \quad (3)$$

Al–Fe–Mn ternary diagrams can be used to distinguish non-hydrothermal silica from hydrothermal silica (see Adachi et al., 1986; Arsairai et al., 2016). Sageman and Lyons (2004) suggest that biogenic and aeolian silica can be distinguished by considering depositional environment, studying sedimentary textures, and by comparison with other elemental proxies. For example, the presence of biogenic silica is supported if the Zr/Al and Ti/Al profiles, which are interpreted to reflect the proportion of continental input, do not correspond to Si/Al peaks (Turner et al., 2015, 2016; Gambacorta et al., 2016). Similarly, Zhang et al. (2019) suggest that corresponding peaks in both Si/Al and Si/Ti indicate that excess silica is more likely biogenic than detrital. Petrographic analysis and scanning electron microscopy with associated imaging techniques (e.g., cathodoluminescence or charge contrast imaging) can also be used to differentiate biogenic silica and detrital quartz (e.g., Schieber et al., 2000; Buckman et al., 2017).

Planktonic organisms can also have calcareous rather than siliceous skeletons (e.g., coccoliths, foraminifera). Several authors have proposed that lithological cycles observed in successions dominated by pelagic carbonates, marlstones, and mudstones are related to variations in relative sea level (e.g., Elder et al., 1994; Dean and Arthur, 1998; Hart, 2015). More specifically, Hart (2015) proposed that pelagic carbonate content increases upwards through transgression to the maximum flooding surface and then decreases upwards during regression. $CaCO_3$ or calcite profiles have been used in conjunction with other datasets (e.g., sedimentological, petrophysical) to identify cycles in some of these studies (e.g., Dean and Arthur, 1998; Hart, 2015) suggesting that Ca could potentially be used as a proxy for pelagic carbonate if this relationship is first confirmed through comparison to XRD and sedimentological datasets.

2.6. Additional influences on composition

A number of factors can influence elemental distributions other than environmental conditions at the time of deposition (Pearce et al., 2005). These include; provenance, bioturbation, post-depositional re-oxidation, diagenesis, oil generation and expulsion, and chemical weathering of outcrops. For example, although Th/U can be a paleoredox indicator (Myers and Wignall, 1987; Wignall and Twitchett, 1996; Kimura and Watanabe, 2001; Sano et al., 2013), it can also vary based on provenance and sedimentary recycling (McLennan et al., 1993). Similarly, trends in Zr/Nb can indicate grain size variations (e.g., Ratcliffe et al., 2006; Sano et al., 2013) or changes in sedimentary provenance, with higher Zr/Nb resulting from an increased proportion of zircon derived from a mature, recycled sedimentary provenance (Ratcliffe et al., 2006).

Bioturbation also affects trace element distribution. Using elemental maps obtained by synchrotron rapid scanning X-ray fluorescence, Harazim et al. (2015) observed partitioning of trace elements (e.g., Cr, V, and Zr) between burrows and burrow halos in Cretaceous continental mudstone samples, which was interpreted to have been caused by mechanical sorting of grains by the trace maker. In marine sedimentary rocks, elemental distributions have also been shown to be heavily impacted by the presence of bioturbation (e.g., Over, 1990). This highlights the importance of understanding the scale and distribution of bioturbation in the interval of interest and assessing geochemical heterogeneity caused by animal-sediment interactions where possible.

Many major and trace elements may be affected by diagenesis, and some elements are more prone to diagenetic remobilization than others (Pearce et al., 1999). For example, of elements often associated with detrital input (e.g., Al, Ti) are effectively immobile during diagenesis (e.g., Thomson et al., 1998; Brumsack, 2006; Tribovillard et al., 2006), although the observation of authigenic kaolinite in the Cretaceous Mancos Shale suggests that Si and Al can be mobile on at least a local scale (Taylor & Macquaker, 2014). Silica can be released during diagenesis through clay mineral transformations (e.g., smectite to illite or illite to muscovite) or through dissolution of silicate minerals or biogenic silica (Schieber, 1996; Taylor & Macquaker, 2014). The observation of early diagenetic quartz suggests that the low permeability and low diffusion coefficients of mudstone intervals prevents significant diagenetic mobility of silica (Taylor & Macquaker, 2014 and references therein). Similarly, K can be incorporated into clays during illitization, whereby a precursor smectite phase can be altered through pore-water enrichment in K^+. Two main mechanisms for smectite to illite transformation have been inferred, including the dissolution of the smectite lattice and growth of illite crystals due to the Ostwald ripening-like effect (Nadeau et al., 1985) and a biological role in which sedimentary microbes concentrated K^+ into their biomass which then becomes liberated during heterotrophic degradation (Aubineau et al., 2019).

Post-depositional diffusion of O_2 into bottom sediments, which can occur in situations such as glacial-interglacial transitions or deposition of turbidites in anoxic settings, leads to re-oxidation of reduced species which can, in turn, result in remobilization of certain elements (Morford et al., 2001; Tribovillard et al., 2006). This has been observed to potentially affect Cr, Mo, Ni, U, and V (e.g., Thomson et al., 1993, 1995; Rosenthal et al., 1995). Tribovillard et al. (2006) suggested that redox-sensitive trace metals associated with sulfides (e.g., Mo, Ni, Re) should be immobile if post-depositional re-oxidation does not occur because sulfides are typically stable during diagenesis in sediments where organic supply is sufficient to support sulfate reduction, and hence sulfide generation.

The enrichment of Ni and V has been observed in oils derived from

type II kerogens (Lewan and Maynard, 1982; Lewan, 1984). This may result in lower than expected enrichment of certain trace metals in organic-rich mudstone units that have undergone oil generation and expulsion (Harris et al., 2013). Chemical weathering also affects composition (Nesbitt and Young, 1982). For example, in a study of two organic-rich mudstone intervals from the Guizhou province in China, Liu et al. (2016) observed the loss of major elements, such as Na, Ca, Mg, Fe, and trace elements, including V and Ni, in outcrop samples compared to core samples. Weathering of organic matter in mudstone intervals has been observed to cause a pronounced breakdown of Ni and V metallo-organic complexes (Grosjean et al., 2004). In a study of the effects of weathering on proxies used for paleoenvironmental interpretation in mudstone successions, Marynowski et al. (2017) observed significant decreases in the concentrations of trace metals including, Mo, Ni, and U, which were attributed to degradation of organic matter and oxidation of pyrite. The depletion of Re from weathering of organic-rich mudstones has also been observed (e.g., Peucker-Ehrenbrink and Hannigan, 2000; Jaffe et al., 2002).

Due to complexities inherent in element and mineral distributions, good practice confirms element affinities using cross plots, comparisons, and statistical analyses. When possible, integrating chemostratigraphic interpretations with other datasets is also recommended (e.g., Algeo et al., 2004; Ver Straeten et al., 2011; Hammes and Frébourg, 2012).

2.7. Normalization to aluminium and the average shale

In many studies, elemental concentrations have been normalized to Al with the aim of accounting for dilution by other components and facilitating comparison between different locations and intervals (Pearce et al., 1999; Van der Weijden, 2002; Algeo et al., 2004; Algeo and Maynard, 2004; Harris et al., 2013). Moreover, elements are normalized to Al in order to compare with average shale values, which then provides an estimate of enrichment of those elements (Brumsack, 2006; Tribovillard et al., 2006). However, Van der Weijden (2002) demonstrated that normalization to Al can result in apparent correlations between unrelated variables or vice versa, especially if the coefficient of variation of Al is large compared to the coefficient of variation of the elements being normalized. Furthermore, Algeo & Lyons (2006) argued that given trace elements and TOC are both affected by dilution, trace metals should not be normalized to Al for comparison with trends in TOC. Finally, understanding the relative proportion and abundance of different elements or minerals is useful for sequence stratigraphy (e.g., identifying condensed sections) and normalizing to Al conflates the dataset. Consequently, normalization to Al should only be performed if the coefficient of variation of Al is similar to that of the element of interest and it is also recommended to consider both normalized profiles and raw profiles. Given its lower solubility, some trace element studies of ancient shales have instead relied on metal/Ti ratios as a proxy for authigenic enrichments (e.g., Reinhard et al., 2013; Fru et al., 2016).

3. Observed chemostratigraphic expression of surfaces

The geochemical expressions of sequence stratigraphic surfaces observed in fine-grained organic-rich intervals are summarized in Table 3.

3.1. Maximum flooding surface

The maximum flooding surface marks the switch from transgression to regression and the time of the maximum landward position of the shoreline (Posamentier and Allen, 1999). A few studies provide examples of the chemostratigraphic expression of this surface. Turner et al. (2016) produced a sequence stratigraphic framework for two outcrops and three cores in the organic-rich Upper Devonian Woodford Shale of the Arkoma Basin, Oklahoma. The third-order maximum flooding surface identified in this interval is characterized by a maximum gamma ray response, relatively high Si/Al, local minimum concentration of terrigenous elements (Al, K, Ti, Zr). This surface also separates underlying strata with lower Mo and V abundance from overlying strata displaying higher Mo and V concentrations (Fig. 3). Higher-frequency surfaces that mark the shift from regression to transgression were recognized chemostratigraphically and are marked by local minima in terrigenous elements (e.g., Al, K, Ti, Zr) and commonly coincide with local maxima in Si/Al and Ca. Turner et al. (2016) refer to these as chemostratigraphic flooding surfaces, herein, these surfaces are interpreted as higher frequency maximum flooding surfaces. Ratcliffe et al. (2012c) and Sano et al. (2013) identified maximum flooding surfaces in the Upper Jurassic Haynesville Shale, an organic-rich mudstone deposited on the slope of a carbonate platform (Frébourg et al., 2013) in a restricted basin setting (Hammes et al., 2011). These studies placed maximum flooding surfaces in the Haynesville Shale at minimums in Zr/Nb, while chemostratigraphic data presented in Sano et al. (2013) also illustrates that maximum flooding surfaces in the Haynesville Shale are characterized by minimums in V abundance (Fig. 4). Data presented in Ratcliffe et al. (2012c) shows that maximum flooding surfaces in this interval typical fall at local lows in terrigenous content. Harris et al. (2018) presented geochemical data for cores from the Duvernay Formation — an organic-rich mudstone deposited in inter-reef settings during the Late Devonian in Alberta (Knapp et al., 2019) — that are included in a previously established sequence stratigraphic framework based on sedimentological and petrophysical attributes. Harris et al. (2018) use the formula for excess Si (Eq. (3)) and interpret all excess Si to be biogenic in origin, potentially because of the presence of siliceous radiolaria in several of the facies observed by Knapp et al. (2017). Maximum flooding surfaces in cores from the West Shale Basin are often near lows in Al and typically correspond to highs in excess Si and Mo/Al. In the East Shale Basin, maximum flooding surfaces are typically near minima in Al, and separate intervals of lower Al with overlying intervals characterized by higher Al abundance. Patterns of excess Si enrichment and Mo/Al do not match those observed in the West Shale Basin, which Harris et al. (2018) attributed to higher carbonate dilution, lower productivity, and higher dissolved oxygenation in the East compared to West Shale Basin.

Results from these studies suggest that maximum flooding surfaces are typically characterized by relatively low levels of terrigenous elements (e.g., Al, K, Ti, Zr), minima in grain size proxies (e.g. Zr/Nb), and maxima in Si/Al (Table 3). The enrichment of redox sensitive trace elements (e.g., Mo, V) at these surfaces appears to be variable. Seeing as maximum flooding surface records a time when continental sediment is stored in landward settings, which is accompanied by the formation of condensed sections in the marine environment (Loutit et al., 1988), a minimum abundance of detrital elements is expected (Turner et al., 2016). In shallow-marine systems, a maximum flooding surface also records the change from fining upwards to coarsening upwards (Embry, 2010). Peaks in Si/Al or excess Si observed by Turner et al. (2015, 2016) and Harris et al. (2018), respectively, were interpreted to reflect a higher proportion of biogenic silica. Both studies observed increases in biogenic silica proxies at maximum flooding surfaces, suggesting that higher biogenic silica content is associated with maximum flooding surfaces, which is also expected in condensed sections (e.g., Bohacs, 1998; Gutierrez Parades et al., 2017). This has been interpreted as the result of increased primary productivity (e.g., Harris et al., 2018), decreased clastic dilution, or a combination thereof (Turner et al., 2016).

Differences in redox sensitive trace metal enrichment associated with maximum flooding surfaces from study to study likely occur because of differences in the paleohydrographic characteristics of the setting. As water depth at a point on the open shelf increases, dissolved oxygen at this location typically declines (Wilde et al., 1996). In modern oceans, consumption of oxygen by degrading organic matter results in the decrease of dissolved oxygen from the surface to a

Table 3
The observed chemostratigraphic expression of sequence stratigraphic surfaces in organic-rich mudstone units.

Sequence stratigraphic surface	Observed chemostratigraphic signature	Examples
Maximum flooding surface	Low abundance of terrigenous proxies	Ratcliffe et al. (2012c), Turner et al. (2015, 2016), Harris et al. (2018)
	Minima in grain size proxies	Ratcliffe et al. (2012c), Sano et al. (2013)
	Increase in proxies for biogenic silica	Turner et al. (2015, 2016), Harris et al. (2018)
	Variable levels of redox proxies depending on paleohydrography	Sano et al. (2013), Turner et al. (2015, 2016), Harris et al. (2018)
Maximum regressive surface	Peak in terrigenous proxies	Ratcliffe et al. (2012c), Harris et al. (2018)
	Peak in grain size proxies	Ratcliffe et al. (2012c), Sano et al. (2013)
	Minima in proxies for biogenic silica	Harris et al. (2018)
	Variable levels of redox proxies depending on paleohydrography	Sano et al. (2013), Harris et al. (2018)

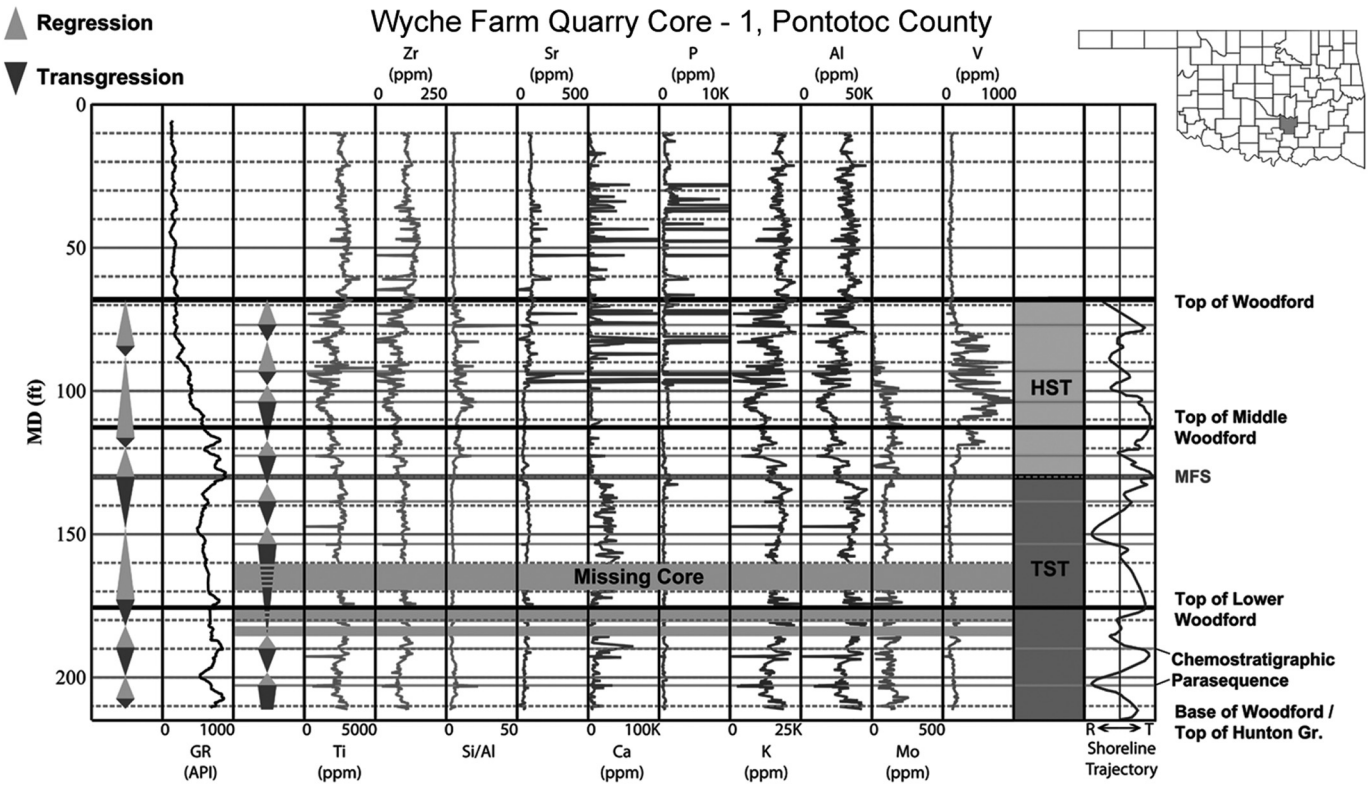

Fig. 3. Chemostratigraphic profiles from the Woodford Formation in the Wyche Farm Quarry Core–1 in Pontotoc County, Oklahoma. Gamma ray log data and chemostratigraphic profiles are presented with the interpreted transgressive-regressive cycles shown to the left of each dataset. The shoreline trajectory shown presents the inferred local shoreline trajectory. The solid grey lines at the change from transgression to regression are herein interpreted as higher frequency maximum flooding surfaces. Acronyms: GR–gamma ray; HST–highstand systems tract; MFS–maximum flooding surface; TST–transgressive systems tract. Reproduced with permission from Turner et al. (2016).

minimum in the zone of lowest circulation (Wyrtki, 1962; Berry and Wilde, 1978). Below this depth, dissolved oxygen increases as a result of ventilation by cold, dense, oxygenated waters produced at high latitudes during the formation of sea ice (Wyrtki, 1962; Berry and Wilde, 1978). The depth of the oxygen minimum can intersect the seafloor from the shelf to the slope (Reichart et al., 1998; Helly and Levin, 2004). At depths near the oxygen minimum, transgression could result in a shift to more oxygenated conditions, whereas for positions well above the oxygen minimum, transgression should lead to a decline in dissolved oxygen. Additionally, transgression can result in rising wave base, causing decreased water column mixing and oxygenation, with the opposite occurring during falling relative sea level (Harris et al., 2013). This change in oxygen is reflected by the ichnofacies model (MacEachern et al., 2009a) with trace fossil assemblages transitioning to those made by organisms more tolerant of suboxic to anoxic conditions as water depth increases and mixing from waves becomes less common resulting in lower dissolved oxygen at the sediment-water interface (MacEachern et al., 2009b; Dashtgard and MacEachern, 2016).

In restricted basin settings, oxygen becomes depleted through decay of organic matter and is not replenished because these basins lack circulation and ventilation (Berry and Wilde, 1978; Schönfeld et al., 2015). If transgression results in increased connectivity to the open ocean, oxygenation can increase from input of ventilated water and improved circulation (Savrda and Bottjer, 1989; Bohacs, 1998). Additionally, Hines et al. (2019) attributed increased bottom water oxygenation during times of transgression to lower productivity, with higher productivity during regression resulting from an increased supply of terrigenous sediment and nutrients. For example, in a study of the Woodford Shale, Turner and Slatt (2016) used Mo/TOC relationships and a decreasing upwards trend in redox-sensitive trace metal enrichment to interpret renewed circulation and decreased basin isolation resulting from transgression. Similarly, Sano et al. (2013) concluded that anoxic conditions during deposition of the Haynesville Shale, which occurred in a restricted intra-shelf basin, prevailed at the onset of transgression. This conclusion has also been made using other datasets. For example, by comparing trace fossil assemblages to organic-carbon and carbonate content in the Upper Cretaceous Niobrara

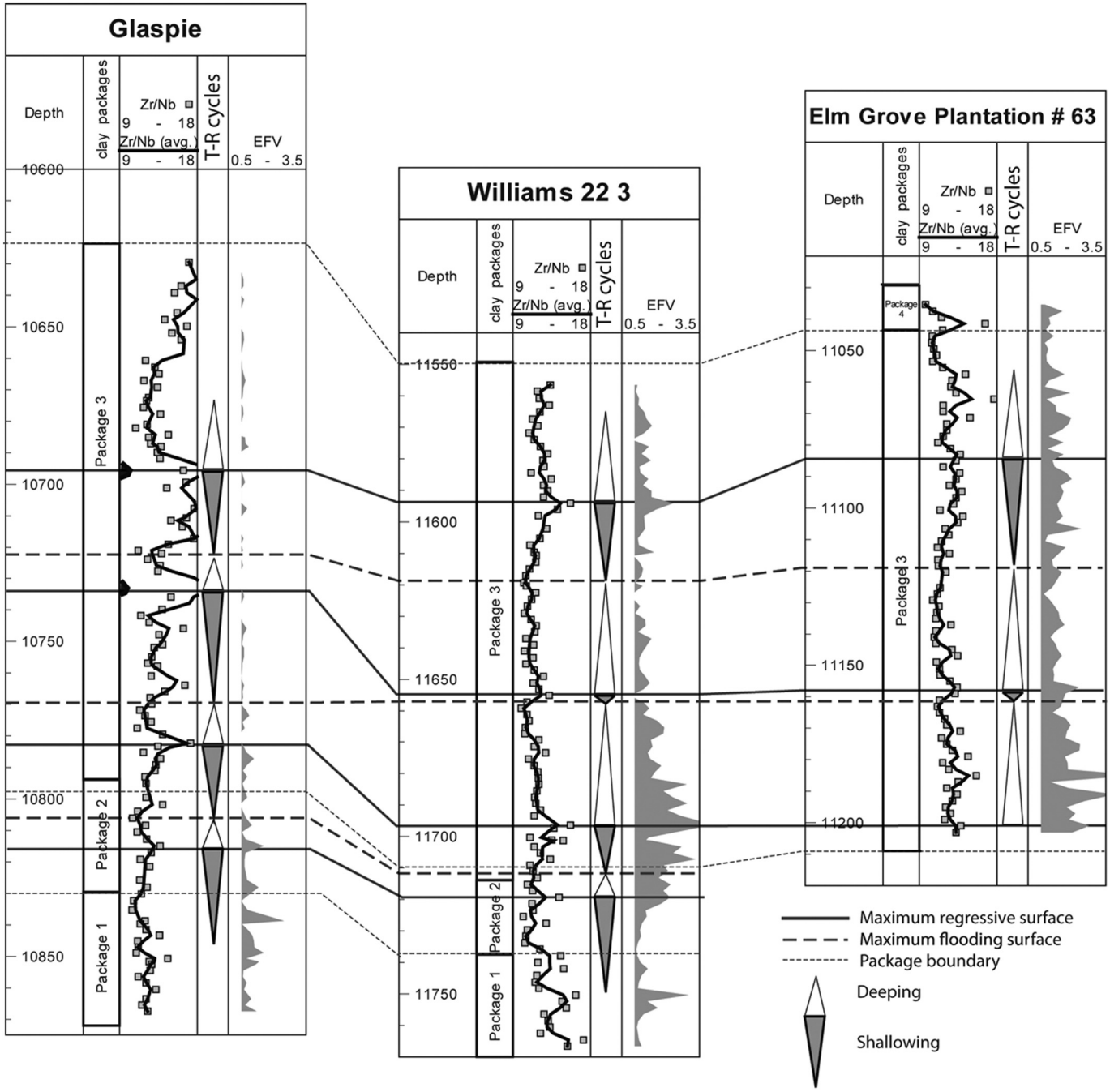

Fig. 4. Chemostratigraphic profiles for the Upper Jurassic strata of three wells in eastern Louisiana and western Texas and associated sequence stratigraphic interpretation. Package 1 corresponds to the Smackover Formation, package 2 comprises the Gilmer Lime Formation, and package 3 and 4 are the Haynesville Formation. The solid Zr/Nb profile represents a moving average with $n = 2$ and the associated squares are the raw data. Acronyms: T-R–transgressive-regressive; EFV–enrichment factor of Vanadium. Reproduced from Sano et al. (2013). Copyright ©2013 by The American Association of Petroleum Geologists. Reprinted by permission of the AAPG whose permission is required for further use.

Formation (Colorado), Savrda and Bottjer (1989) interpreted intervals of increased oxygenation to reflect open marine circulation in the Western Interior Seaway during transgression. Because of differences in the effect of relative sea level on water column oxygenation depending on the setting, the relative enrichment of redox-sensitive trace metals at maximum flooding surfaces depends on whether a shift from transgression to regression resulted in increased or decreased water column oxygenation.

3.2. Maximum regressive surface

The maximum regressive surface occurs at the change from regression to transgression and marks the maximum basinward shoreline position (Helland-Hansen and Martinsen, 1996). Chemostratigraphic examples of maximum regressive surfaces in the Haynesville Shale can be found in Ratcliffe et al. (2012c) and Sano et al. (2013) where they are identified by maxima in Zr/Nb. The terrigenous input profile (sum of Al, K, Na, Ti) plotted by Ratcliffe et al. (2012c) typically displays peaks at maximum regressive surfaces, while the V enrichment profile in Sano et al. (2013) shows that maximum flooding surfaces most often

mark the shift from increasing V enrichment to decreasing V enrichment (Fig. 4). The chemostratigraphic data presented in Harris et al. (2018) shows that the maximum regressive surface identified in the Duvernay Formation West Shale Basin by Knapp et al. (2019) is characterized by relatively high Al, minimum Mo/Al with values near 0, and low levels of biogenic Si.

In marine shelf environments, the maximum regressive surface typically records the shift from coarsening upwards to fining upwards (Catuneanu, 2002; Embry, 2010), which is reflected in these examples by peaks in grain size proxies or detrital elements. Results from Harris et al. (2018) suggest that maximum regressive surfaces are characterized by a low abundance of biogenic silica. As previously discussed, changes in relative sea level can have variable effects on water column oxygenation depending on the setting. The shift from increasing to decreasing V enrichment associated with maximum regressive surfaces in the Haynesville Shale is likely the product of highest levels of basin isolation at this time. Harris et al. (2018) interpreted that times of higher sea level during deposition of the Duvernay Formation were characterized by lower bottom water oxygenation because of reduced water column mixing, high productivity, and inflow of oxygen depleted bottom waters. This implies that minima in Mo/Al associated with the maximum regressive surface in the Duvernay Formation of the West Shale Basin can be explained by highest levels of mixing, lowest productivity, and minimum inflow of oxygen depleted bottom waters.

4. Observed Geochemical Expression of Systems Tracts

The geochemical expressions of systems tracts observed in fine-grained organic-rich intervals are summarized in Table 4.

4.1. Transgressive systems tract

The transgressive systems tract comprises strata deposited when the rate of relative sea-level rise surpasses the rate of shoreline sediment supply (Posamentier and Allen, 1999). Examples of the chemostratigraphic expression of the transgressive systems tract include Turner et al. (2015, 2016), Sano et al. (2013), Ratcliffe et al. (2012c), Hammes & Frebourg (2012), Ver Straeten et al. (2011), and Harris et al. (2018). Turner et al. (2015 and 2016) interpret a third-order transgressive systems tract in the organic-rich Woodford Shale. In this example, the transgressive systems tract is characterized by an overall decline in terrigenous elements (e.g., Ti, Zr, K, Al) and in redox sensitive elements (e.g., Mo, V) reflecting decreasing restriction, and often by increasing Si/Al that arises from an increasing proportion of biogenic silica (Fig. 3). However, in certain intervals, V is concentrated in phosphatic nodules, resulting in V abundance peaks that are not associated with reduced circulation (Turner et al., 2016). Turner et al. (2016) also identified fourth-order T-R cycles based on trends in Ti and Zr with trends of decreasing concentration characterizing transgression.

Other studies focus on the Upper Jurassic Haynesville Shale of Texas and Louisiana. Ratcliffe et al. (2012c) identified lower-frequency T-R cycles in the Haynesville Formation with higher-frequency T-R cycles superimposed on these trends. Higher-rank transgressive packages are characterized by a declining abundance of terrigenous content, which is the sum of Al_2O_3, TiO_2, Na_2O, and K_2O. Lower-rank transgressive intervals are characterized by declining Zr/Nb and SiO_2/Al_2O_3. Trends in Zr/Nb and SiO_2/Al_2O_3 follow one another, indicating that they are associated with the fraction of silt size sediment and that biogenic silica is proportionately less important in the Haynesville Formation (Ratcliffe et al., 2012c). This interpretation is supported by the clear positive trend between Zr and Si observed in the Si–Zr cross plot for the Haynesville Formation (Ratcliffe et al., 2012c). Sano et al. (2013) identified T-R sequences in the same three localities as Ratcliffe et al., 2012c (Fig. 4). In this case, V enrichment data is also presented, and those authors interpreted that anoxia decreases throughout transgression.

Hammes & Frebourg (2012) also studied the Haynesville Shale. In this dataset, the transgressive systems tract is expressed by lower Al concentration than the overlying highstand systems tract. In contrast, Si/Al, Ti/Al, and Zr/Al are elevated compared to the overlying highstand systems tract. The authors contended that an increased abundance of Ti and Zr supports the interpretation that bottom waters were euxinic because they are redox sensitive elements. With that said, Ti and Zr are generally taken to reflect detrital input (Bhatia and Crook, 1986; Plank and Langmuir, 1998; Piper and Calvert, 2009), and have not been shown by previous studies to be redox sensitive. The opposite

Table 4
The observed chemostratigraphic expression of systems tracts in fine-grained organic-rich intervals.

Systems tract	Observed chemostratigraphic signature	Examples
TST	Decreasing Al	Hammes & Frebourg (2012), Ver Straeten et al. (2011),Turner et al. (2015, 2016), Harris et al. (2018)
	Decreasing sums of terrigenous elements (e.g., Al + Ti + Na + K)	Ratcliffe et al. (2012c)
	Variable trends in elements associated with heavy minerals (Ti and Zr):	
	Decreases	Ver Straeten et al. (2011), Turner et al. (2016)
	Increases	Hammes & Frebourg (2012), Ver Straeten et al. (2011)
	Decreasing grain size proxies	Ratcliffe et al. (2012c), Sano et al. (2013)
	Elevated proxies for biogenic silica	Turner et al. (2015, 2016), Harris et al. (2018)
	Variable levels of redox proxies depending on paleohydrography	Hammes & Frebourg (2012), Ver Straeten et al. (2011), Sano et al. (2013), Turner et al. (2015, 2016), Harris et al. (2018)
HST	Increasing Al	Hammes & Frebourg (2012), Turner et al. (2015, 2016), Harris et al. (2018)
	Variable trends in elements associated with heavy minerals (Ti and Zr):	
	Decreases	Hammes & Frebourg (2012)
	Increases	Turner et al. (2015, 2016)
	Variable levels of biogenic silica proxies	Harris et al. (2018)
	Variable levels of redox proxies depending on paleohydrography	Turner et al. (2015, 2016), Harris et al. (2018)
RST	Increasing Al	Turner et al. (2015, 2016), Ver Straeten et al. (2011)
	Variable trends in elements associated with heavy minerals (Ti and Zr):	
	Decreases	Ver Straeten et al. (2011)
	Increases	Turner et al. (2015, 2016), Ver Straeten et al. (2011)
	Increasing grain size proxies	Ratcliffe et al. (2012c), Sano et al. (2013)

Abbreviations: TST–transgressive systems tract; HST–highstand systems tract; RST–regressive systems tracts.

trends in the Al profile compared to the Si/Al, Ti/Al, and Zr/Al suggest decoupling between the sources of Al versus Si, Ti, and Zr, which could potentially occur if Si, Ti, and Zr are primarily associated with the wind-blown detrital fraction. Hammes & Frebourg (2012) did propose that the detrital fraction in the transgressive strata is likely primarily aeolian. The Mo enrichment profile is also elevated compared to the overlying highstand systems tract.

Ver Straeten et al. (2011) identified third-order transgressive systems tracts in the Middle Devonian Oatka Creek and Skaneateles formations deposited in the Appalachian Basin in western New York during the Middle Devonian. These formations are both included in the Hamilton Group and the Oatka Creek Formation is also a member of the Marcellus Subgroup (Arthur and Sageman, 2005). At this location, the Oatka Creek Formation dominantly comprises organic-rich shale with a few limestone interbeds and is interpreted to reflect deposition in primarily anoxic conditions (Ver Straeten et al., 2011). In this interval, the transgressive systems tract is characterized by a small decrease in Al and Ti/Al, and stable levels of Si/Al in the organic-rich mudstone intervals. This systems tract also shows markedly lower Mo abundance than the overlying regressive strata, suggesting a restricted depositional setting with increased connectivity to the open ocean in the transgressive systems tract. The Appalachian Basin was a restricted epicratonic basin (Rowe et al., 2008) and, therefore, increased oxygenation accompanying the transgressive systems tract is expected. The overlying Skaneateles Formation is composed primarily of interbedded mudstone and organic-rich mudstone and was deposited in a dominantly suboxic environment (Ver Straeten et al., 2011). In this formation, the transgressive systems tract is expressed chemostratigraphically by overall low Mo, which is expected in a suboxic interval. Here the transgressive systems tract also shows a significant decrease in Al while Ti/Al and Si/Al show increasing trends that are opposite to trends in Al. Ver Straeten et al. (2011) suggested that increasing Ti/Al and Si/Al can be attributed to elevated levels of silica from aeolian or volcanic sources. Data presented by Harris et al. (2018) shows that transgressive systems tracts in the Devonian Duvernay Formation of the West Shale Basin in Alberta are characterized by decreasing Al_2O_3, rising excess Si, and elevated Mo/Al.

Together, the aforementioned studies suggest that the geochemical signature of a transgressive systems tract includes decreasing Al (Table 4). Other elements associated with detrital minerals (e.g., Ti, Zr) may also decrease (e.g., transgressive systems tract in the Oatka Creek Formation presented in Ver Straeten et al., 2011; Turner et al., 2016), and composite profiles of terrigenous elements may show declining trends (e.g., the terrigenous input profile of Ratcliffe et al., 2012c). Although in some instances, certain detrital elements (e.g., Ti, Zr) show increasing trends (e.g., transgressive systems tract in the Skaneateles Formation of Ver Straeten et al. (2011); Hammes & Frebourg, 2012). During a transgression, sediment trapping in fluvial and/or coastal environments while the shoreline moves landward results in a decrease in the abundance of fluvial detrital sediment that reaches the shelf and slope (Loutit et al., 1988; Mann and Stein, 1997; Catuneanu, 2006). This is likely the cause for the observed decreases in the abundance of Al and of other terrigenous elements where they occur. Turner et al. (2016) observed stronger declines in elements associated with heavy minerals (e.g., Ti and Zr) compared to elements associated with clay minerals (e.g., Al and K) and proposed that this is explained by terrestrial heavy minerals settling out sooner than clay minerals. Increases in Ti/Al and Zr/Al observed in certain cases may be the product of increased aeolian or volcanic input as suggested by Ver Straeten et al. (2011). In marine shelf environments, transgressions are also typically characterized by fining-upwards grain size trends (Catuneanu et al., 2009; Embry, 2010), reflected by declining Zr/Nb and Si/Al in Haynesville Formation (e.g., Ratcliffe et al., 2012c; Sano et al., 2013).

These studies all display elevated proxies for excess silica during transgressive systems tracts. In certain cases, this was interpreted as biogenic silica (e.g., Turner et al., 2016; Harris et al., 2018). Condensed sections develop because of a decline in the abundance of terrigenous sediment input during transgression (Loutit et al., 1988; Galloway, 1989). The proportion of biogenic sediment increases in these intervals as dilution from detrital sediment declines (Arthur and Sageman, 2005; Ver Straeten et al., 2011). High levels of biogenic silica in transgressive systems tracts can also be interpreted as the product of increased biological productivity (e.g., Harris et al., 2018). Ver Straeten et al. (2011) interpreted that rising levels of Si/Al and Ti/Al in the transgressive systems tract of the Skaneateles Formation likely reflects higher aeolian or volcanic input.

Trends in redox sensitive trace metal enrichment through the transgressive systems tract are variable. Certain studies show decreasing paleoredox proxies (e.g., Sano et al., 2013; Ver Straeten et al., 2011; Turner et al., 2016), whereas others show increases (e.g., Hammes & Frebourg, 2012; Harris et al., 2018), likely because of differences between the paleohydrographic conditions of each depositional setting.

4.2. Highstand systems tract

Strata of the highstand systems tract are deposited when the rate of relative sea-level rise decreases such that the rate of sediment supply equals or exceeds the rate of accommodation generation at the shoreline (Posamentier and Allen, 1999). Examples of the geochemical expression of highstand systems tract deposits were presented by Turner et al. (2015, 2016) where they interpreted a third-order highstand systems tract at the top of the Woodford Shale characterized by increasing Ti, Zr, Al, and K, decreasing Si/Al, and relatively low Mo and V (Fig. 3). Similarly, Hammes and Frebourg (2011) suggested that the organic-rich Upper Jurassic Bossier Formation (Texas and Louisiana) records a second-order highstand systems tract, characterized by increasing Al upwards, and decreasing Si/Al, Ti/Al, and Zr/Al. Highstand systems tracts in the Duvernay Formation of the West Shale Basin show increasing Al. In this example, Mo/Al typically remains elevated moving from the maximum flooding surface until the mid-highstand systems tract, where it then begins to decline. The lowermost highstand systems tract exhibits decreasing biogenic Si, but subsequent highstand systems tract record continuing elevated levels of excess Si following transgressive systems tracts (Harris et al., 2018). It is important to note that the highstand systems tracts in all of the above examples were identified based on other datasets. At this point, criteria to identify the highstand systems tract chemostratigraphically are poorly constrained because no geochemical signature for the basal surface of forced regression has been defined. Nonetheless, in some cases it is possible to identify the highstand, falling-stage, and lowstand systems tracts in fine-grained unconventional plays using other datasets such as seismic (e.g., Dominguez and Catuneanu, 2017).

The highstand systems tracts described above are all characterized by increasing Al content, likely reflecting progradation associated with relative sea level highstand. Titanium and Zr also increase in some instances and stable Ti/Al observed in one case likely reflects proportional increases in both Ti and Al. However, Zr/Al and Ti/Al decline throughout the highstand systems tracts in other studies, potentially due to falling aeolian or volcanic input. Decreasing Si/Al interpreted as declining biogenic silica moving upwards through highstand systems tracts is likely the product of higher dilution by detrital sediment or lower productivity. Conversely, increases in proxies for biogenic silica (e.g., Si/Al, excess Si) through the highstand systems tract can be interpreted as continuing elevated levels of biological productivity (e.g., Harris et al., 2018). The signature of redox proxies through the highstand systems tract depends on paleohydrographic conditions. For example, low levels of Mo and V observed by Turner et al. (2016) during a highstand systems tract in the Woodford Shale were interpreted as the product of greater oxygenation caused by a higher degree of connectivity between the Arkoma Basin and the Palaeotethys at this time. Harris et al. (2018) suggested that the Mo/Al patterns observed in

highstand systems tracts of the Duvernay Formation in the West Shale Basin are attributed to higher input of anoxic nutrient-rich seawater from lower basin restriction leading to higher productivity and more reducing conditions during the upper transgressive systems tracts and lower highstand systems tracts.

4.3. Regressive systems tract

The regressive systems tract constitutes all strata deposited when the shoreline moves basinward (Embry, 2002; Embry and Johannessen, 1993). The regressive systems tract includes strata of the highstand, falling-stage, and lowstand systems tracts (Catuneanu, 2002). Turner et al. (2015 and 2016) interpreted fourth-order regressive systems tracts superimposed on third-order trends in the Woodford Shale based on Ti and Zr profiles, which displayed similar signatures to trends in K and Al. These regressive intervals are typically characterized by increasing Ti, Zr, K, and Al (Fig. 3). Lower rank regressive systems tracts are interpreted in the Haynesville Shale by Ratcliffe et al. (2012c) and Sano et al. (2013). These regressive trends are characterized by increasing Zr/Nb and Si/Al in Ratcliffe et al. (2012c) and increasing Zr/Nb and V in Sano et al. (2013); Fig. 4). Ratcliffe et al. (2012c) interprets that Zr/Nb and Si/Al record grain size variations in the Haynesville Formation. Ver Straeten et al. (2011) presented geochemical profiles along with a previously established sequence stratigraphic interpretation for the Devonian Oatka Creek and Skaneateles formations. They use the term 'early highstand systems tract' for the highstand systems tract and the term 'late highstand systems tract' rather than 'falling-stage systems tract' for the interval deposited during relative sea level fall, following the Van Wagoner et al. (1988) model. In their interpretations, these are grouped together as the highstand systems tract rather than separated into the early highstand systems tract and late highstand systems tract. Ver Straeten et al. (2011) suggested that lowstand systems tracts are not present above these highstand systems tracts but are instead overlain by transgressive systems tracts. These highstand systems tracts are herein considered as regressive systems tracts as they may include both normal and forced regressive deposits. The third-order regressive systems tract in the Oatka Creek Formation is characterized by increasing Al, decreasing Si/Al, and Ti/Al, and a marked increase in Mo relative to the underlying transgressive systems tract. The regressive systems tract in the overlying Skaneateles Formation displays rising Al and Si/Al, with relatively stable Ti/Al. Molybdenum remains quite low through the entire interval.

These studies suggest that regressive systems tracts are typically characterized by an increasing abundance of detrital elements and grain size proxies reflecting ongoing progradation. An exception to this is present in the regressive systems tract of the Oatka Creek Formation, where Si/Al and Ti/Al decline, which Ver Straeten et al. (2011) interpreted to have been caused by falling levels of aeolian input.

5. Discussion

To our knowledge, there are no existing examples of the chemostratigraphic expression of certain surfaces. These include the subaerial unconformity, correlative conformity, transgressive surface of erosion, regressive surface of marine erosion, and basal surface of forced regression. The subaerial unconformity is the unconformable portion of the surface that marks the end of forced regression and is typically developed in shelf or platform settings (Hunt and Tucker, 1992). This surface is defined by non-marine strata on top (Catuneanu, 2006; Shanmugam, 1988) and is not relevant to the marine mudstone successions discussed in this work. As the concept of integrating chemostratigraphic datasets for sequence stratigraphy is fairly recent, there are relatively few studies that have compared elemental proxies to previously established sequence stratigraphic frameworks or used chemostratigraphy to help identify surfaces. The recognition of sequence stratigraphic cyclicity within mudstone units is also relatively new (e.g., Bohacs and Schwalbach, 1992; Macquaker and Taylor, 1996; Bohacs, 1998; Schieber, 1998; Williams et al., 2001; Bohacs et al., 2005; Macquaker et al., 2007). For these reasons, it is not yet possible to define the chemostratigraphic expression of the correlative conformity and basal surface of forced regression. During a transgression, the transgressive surface of erosion forms from erosion by waves or tides (Swift, 1975; Catuneanu, 2002), and typically forms in coastal and upper shoreface settings (Catuneanu, 2002). Similarly, the regressive surface of marine erosion is cut by waves during forced regression (Plint and Nummedal, 2000) and this erosion takes place on the inner shelf (Plint and Nummedal, 2000; Catuneanu, 2002). Until recently, fine-grained organic-rich successions were viewed as largely distal, deep-water deposits, which would suggest that the transgressive surface of erosion and regressive surface or marine erosion are not relevant to these units. However, many organic-rich mudstone successions are now being re-interpreted to reflect deposition in more proximal environments than originally thought (e.g., Schieber, 1994; Smith et al., 2019). This may lead to increased recognition of these surfaces and allow for future delineation of their chemostratigraphic characteristics.

Flooding surfaces and parasequences are not discussed in this work. A flooding surface (i.e., parasequence boundary) records an abrupt water deepening (Van Wagoner et al., 1988), which may or may not record a change in stratal stacking pattern (Catuneanu, 2019a); as such, it is a surface of allostratigraphy rather than sequence stratigraphy (Catuneanu, 2019a). Certain studies of mudstone intervals still make use of flooding surfaces and parasequences rather than lower rank sequence stratigraphic surfaces and sequences (e.g., Bohacs et al., 2014; Birgenheier et al., 2017; Borcovsky et al., 2017; Turner et al., 2015, 2016), even though the parasequence boundaries no longer comply with the original definition of a flooding surface. Therefore, following Catuneanu (2019a), this paper recommends that the use of scale-independent terminology (i.e., the recognition of higher-frequency sequence stratigraphic surfaces and systems tracts) provides a superior alternative for stratigraphic mapping and correlation than the delineation of parasequences (see Catuneanu, 2019a, for a full discussion).

The chemostratigraphic expression of lowstand systems tracts and falling-stage systems tracts have not yet been established, likely for similar reasons as discussed for the basal surface of forced regression and correlative conformity. Additionally, although all systems tracts may be present, higher frequency cycles identified using chemostratigraphic profiles in these units are commonly limited to the identification of transgression and regression rather than parsing out normal from forced regressions (e.g., Ratcliffe et al., 2012c; Sano et al., 2013; Turner et al., 2015, 2016). As a result, only two systems tracts are commonly recognized: the transgressive systems tract and regressive systems tract. This is likely the case because in shelfal settings the regressive systems tract records ongoing progradation, making the basal surface of forced regression and correlative conformity cryptic in studies using log, core, or outcrop data (Catuneanu, 2006). This, therefore, leads to difficulty in distinguishing the highstand systems tract, lowstand systems tract, and falling-stage systems tract in these settings. It is also possible that certain systems tracts are not developed in particular depositional settings.

One disadvantage of using an undifferentiated regressive systems tract is that it amalgamates different genetic types of regressive strata, which lowers the resolution of the sequence stratigraphic study. Considering normal and forced regressive deposits together may also be disadvantageous if they have different characteristics related to their unconventional reservoir potential, for example variations in TOC have been recorded between forced vs. normal regressive systems tracts in unconventional plays (Dominguez et al., 2016; Dominguez and Catuneanu, 2017). These are limitations of using chemostratigraphic datasets to identify sequence stratigraphic cycles in fine-grained organic-rich units.

The geochemical characteristics of sequence stratigraphic surfaces and systems tracts in organic-rich mudstone intervals are expected to

vary depending on the depositional setting. For example, based on comparison with coarser grained intervals, we expect that there are differences between the chemostratigraphic expression of certain surfaces in more proximal settings influenced by progradation compared to more distal settings beyond the influence of progradation where sediment-gravity deposition and pelagic sedimentation are dominant. Examples of environments influenced by progradation are the continental shelf or a ramp setting under the influence of shoreline progradation. The slope or abyssal plain of a shelf-slope system or a ramp setting where sedimentation is dominated by sediment-gravity flows and pelagic fallout are examples of settings that are beyond the influence of shoreline progradation. Herein, environments experiencing progradation will be referred to as shallow-water settings, whereas settings beyond the influence of progradation where sedimentation is dominated by sediment-gravity flows and pelagic settling will be referred to as deep-water settings. During relative sea-level fall, the deep-water environment experiences maximum supply of detrital sediment, and the detrital sediment supplied to these settings is coarser than the sediment that accumulates during relative sea-level rise (Posamentier and Kolla, 2003). Unlike for prograding environments, deposition in deep-water is less predictable in terms of the locus of accumulation of depositional elements. However, general trends can still be established at the scale of composite profiles that integrate regional data (e.g., fig. 36 in Catuneanu, 2019b). The main contrasts between the shallow- and deep-water settings are recorded by the grain-size changes associated with the correlative conformity and the maximum regressive surface. In shallow-water environments, the correlative conformity is more difficult to distinguish because it occurs within a prograding and coarsening upwards interval (Catuneanu, 2006), whereas the maximum regressive surface marks the change from coarsening to fining upwards grain size trends (Catuneanu, 2002; Embry, 2010). In coarser grained deep-water intervals dominated by sediment-gravity flows, the composite vertical profile coarsens upwards to the correlative conformity during relative sea-level fall, and then fines upwards through the lowstand systems tract to the maximum flooding surface (Catuneanu, 2006, 2019a). In this case, the maximum regressive surface is present within a fining upwards interval and is more difficult to distinguish (Catuneanu, 2019b). These trends relate to the efficiency of transfer of fluvial sediment across the shelf to the deep-water setting, which is highest during forced regression (see full discussion in Catuneanu, 2019a, 2019b). We expect that this would affect the chemostratigraphic signatures of the correlative conformity and maximum regressive surface in organic-rich mudstone units depending on the setting, with the maximum regressive surface recording maxima in terrigenous proxies and grain size proxies in shallow-water settings, but the correlative conformity recording these maxima in deep-water settings, although this has not yet been confirmed. The examples discussed herein seem to correspond to the expected expression of the maximum regressive surface in settings influenced by progradation. Further work is required to provide examples of the chemostratigraphic expression of these surfaces and systems tracts in shallow- versus deep-water settings so that the chemostratigraphic expression can be confirmed.

In chemostratigraphic studies of mudstone successions, geochemical composition data is typically collected using either inductively coupled plasma (ICP) and inductively coupled plasma mass spectrometry (ICP-MS) or inductively coupled plasma optical emission spectrometry (ICP-OES) (e.g., Harris et al., 2013, 2018; Sano et al., 2013; Playter et al., 2018), or by portable energy-dispersive X-ray fluorescence (pXRF) (e.g., Hammes and Frébourg, 2012; Sano et al., 2013; Turner et al., 2015, 2016; El Attar and Pranter, 2016; Hines et al., 2019). Advantages of pXRF compared to ICP methods include time and cost efficiency as well as the non-destructive nature of the analysis, potentially allowing for the collection of higher-resolution datasets (Rowe et al., 2012; Rowe et al., 2017; Lemiere, 2018; Zhang et al., 2019). There are, however, some drawbacks associated with pXRF, including a more limited suite of elements that can be obtained compared to ICP analyses (Rowe et al., 2017), and for certain elements, poor accuracy relative to accepted values or concentrations obtained by other laboratory-based analyses (e.g., Rowe et al., 2012; Hines et al., 2019). The use of helium flow or high-performance detectors is now allowing for measurement of lighter elements (e.g., Al and Si), which were traditionally poorly detected by pXRF, although lower accuracy has been reported for Al compared to elements such as Si, Ti, and in some cases, Zr (Lemiere, 2018). Nonetheless, in a study specific to mudstone intervals, Rowe et al. (2012) observed high accuracy for Al and Si. Of the other elements discussed herein, Rowe et al. (2012) observed less reliable Cr pXRF measurements when concentrations were below 70 ppm, and unreliable U and Th results when pXRF data was compared to data collected using wavelength dispersive x-ray fluorescence. Uranium can be difficult to measure with XRF because of inter-element interference and low abundance in many samples (Rowe et al., 2017), and along with Zr, Cr, and Ni, U is one of the elements for which Hines et al. (2019) observed poor correlations between pXRF data and other laboratory-based measurements (fusion XRF and ICP-MS).

An additional drawback related to the integration of chemostratigraphic datasets for sequence stratigraphic interpretation is the requirement for fairly continuous measurements from core or outcrop intervals in order to identify surfaces (Pearce et al., 2010). For example, studies that identified sequence stratigraphic surfaces and systems tracts (e.g., Ver Straeten et al., 2011; Sano et al., 2013; Turner et al., 2016) sampled cores and outcrops at intervals ranging from 5 to 120 cm. These high-resolution sampling rates are not possible when relying on drill cuttings rather than core and outcrop samples because drill cuttings are typically taken at coarser intervals (Pearce et al., 1999). Given the limitations associated with the use of chemostratigraphic datasets, chemostratigraphy is more effective when used in conjunction with other datasets (e.g., sedimentological and petrophysical) to form robust sequence stratigraphic frameworks in organic-rich mudstone intervals (e.g., Ver Straeten et al., 2011; Hammes and Frébourg, 2012).

6. Conclusions

This review of documented elemental stratigraphic changes in marine mudstone successions and their interpretation allows for a preliminary delineation of the chemostratigraphic expression of certain sequence stratigraphic surfaces and systems tracts, namely the maximum flooding surface, maximum regressive surface, transgressive systems tract, and regressive systems tract. Chemostratigraphic characteristics of the highstand systems tract are presented, although this systems tract has been identified using criteria other than chemostratigraphic in all examples presented in this work, and presently cannot be distinguished from the regressive systems tract based on chemostratigraphic proxies alone. Available sequence stratigraphic interpretations of geochemical proxy datasets presented herein demonstrate that chemostratigraphic datasets are quite useful in interpreting transgressive-regressive cycles (regressive systems tracts and transgressive systems tracts separated by maximum regressive surfaces and maximum flooding surfaces, respectively). Also apparent is the need for integration with other datasets to further subdivide the regressive systems tract and confirm proxy signatures to produce robust sequence stratigraphic frameworks. To date, the utility of incorporating chemostratigraphic datasets for the study of sequence stratigraphic cyclicity in organic-rich mudstone successions has been demonstrated by a handful of studies. Nonetheless, the field remains quite new with limited published examples of the geochemical expression of surfaces and systems tracts. Furthermore, because of the lack of consensus and ongoing shift in our understanding of mudstone depositional systems, it is not yet possible to confirm many of the expected differences in the chemostratigraphic expression of surfaces and systems tracts depending on the depositional setting. The following are suggestions aimed at advancing the field. First, the publication of studies comparing

geochemical proxies to previously established sequence stratigraphic frameworks (based on other datasets) for fine-grained organic-rich intervals will enable further geochemical characterization of surfaces and systems tracts and allow chemostratigraphy to be better integrated with other datasets. Incorporating chemostratigraphic datasets while developing sequence stratigraphic interpretations in organic-rich intervals where these frameworks do not yet exist will serve a similar purpose. As our understanding of depositional systems for these units increases, characterizing the differences in chemostratigraphic expression of surfaces and systems tracts associated with variations in depositional setting will also further the utility of chemostratigraphic data to sequence stratigraphic studies of mudstone successions.

Declaration of competing interest

None.

Acknowledgments

The authors would like to thank Kathryn Fiess, Viktor Terlaky, Dave Herbers, Carolyn Furlong, and Sara Biddle for their advice and guidance. Maya LaGrange, Brette Harris, and Murray Gingras acknowledge the Northwest Territories Geological Survey for generously providing funding of this work. Kurt Konhauser, Octavian Catuneanu, and Murray Gingras thank the Natural Sciences and Engineering Research Council of Canada (NSERC) for their financial support. We would also like to thank the editor Chris Fielding and reviewers Bruce Hart, Bryan Turner, and Lauren Birgenheier for providing feedback that greatly improved the quality of the manuscript.

References

Adachi, M., Yamamoto, K., Sugisaki, R., 1986. Hydrothermal chert and associated siliceous rocks from the northern Pacific their geological significance as indication of ocean ridge activity. Sediment. Geol. 47 (1-2), 125–148.

Algeo, T.J., Lyons, T.W., 2006. Mo–total organic carbon covariation in modern anoxic marine environments: Implications for analysis of paleoredox and paleohydrographic conditions. Paleoceanography 21 (1), PA1016.

Algeo, T.J., Maynard, J.B., 2004. Trace-element behavior and redox facies in core shales of Upper Pennsylvanian Kansas-type cyclothems. Chem. Geol. 206 (3–4), 289–318.

Algeo, T.J., Schwark, L., Hower, J.C., 2004. High-resolution geochemistry and sequence stratigraphy of the Hushpuckney Shale (Swope Formation, eastern Kansas): implications for climato-environmental dynamics of the Late Pennsylvanian Midcontinent Seaway. Chem. Geol. 206 (3–4), 259–288.

Arsairai, B., Wannakomol, A., Feng, Q., Chonglakmani, C., 2016. Paleoproductivity and paleoredox condition of the Huai Hin Lat Formation in northeastern Thailand. J. Earth Sci. 27 (3), 350–364.

Arthur, M.A., Sageman, B.B., 2005. Sea-level control on source-rock development: perspectives from the Holocene Black Sea, the mid-Cretaceous Western Interior Basin, and the late Devonian Appalachian basin. In: Harris, N.B. (Ed.), The Deposition of Organic-Carbon-Rich Sediments: Models, Mechanisms, and Consequences: Society of Economic Paleontologists and Mineralogists Special Publication. 82. pp. 35–59.

Aubineau, J., El Abani, A., Bekker, A., Somogyi, A., Bankole, O.M., Macchiarelli, R., Meunier, A., Riboulleau, A., Reynaud, J.-Y., Konhauser, K.O., 2019. Microbially induced potassium enrichment in Paleoproterozoic shales and implications for reverse weathering on early Earth. Nat. Commun. 10 (1), 1–9 2670.

Berry, W.B., Wilde, P., 1978. Progressive ventilation of the oceans; an explanation for the distribution of the lower Paleozoic black shales. Am. J. Sci. 278 (3), 257–275.

Bhatia, M.R., Crook, K.A., 1986. Trace element characteristics of graywackes and tectonic setting discrimination of sedimentary basins. Contrib. Mineral. Petrol. 92, 181–193.

Birgenheier, L.P., Horton, B., McCauley, A.D., Johnson, C.L., Kennedy, A., 2017. A depositional model for offshore deposits of the lower Blue Gate Member, Mancos Shale, Uinta Basin, Utah, USA. Sedimentology 64 (5), 1402–1438.

Bloemsma, M.R., Zabel, M., Stuut, J.B.W., Tjallingii, R., Collins, J.A., Weltje, G.J., 2012. Modelling the joint variability of grain size and chemical composition in sediments. Sediment. Geol. 280, 135–148.

Bohacs, K.M., 1998. Contrasting expressions of depositional sequences in mudrocks from marine to non-marine environs. In: Schieber, J., Zimmerle, W., Sethi, P.S. (Eds.), Shales and Mudstones: Volume I. E. Schweizerbart'sche Verlagsbuchhandlung (Nägele u. Obermiller), Stuttgart, pp. 33–78.

Bohacs, K.M., Schwalbach, J.R., 1992. Sequence stratigraphy of fine-grained rocks with special reference to the Monterey Formation. In: Schwalbach, J.R., Bohacs, K.M. (Eds.), Sequence Stratigraphy in Fine-Grained Rocks: Examples from the Monterey Formation, pp. 7–19 Pacific Section, Society of Economic Paleontologists and Mineralogists, Book 70.

Bohacs, K.M., Grabowski Jr., G.J., Carroll, A.R., Mankiewicz, P.J., Miskell-Gerhardt, K.J., Schwalbach, J.R., Wegner, M.B., Simo, J.T., 2005. Production, destruction, and dilution—the many paths to source-rock development. In: Harris, N.B. (Ed.), The Deposition of Organic-Carbon-Rich Sediments: Models, Mechanisms, and Consequences: Society of Economic Paleontologists and Mineralogists Special Publication. 82. pp. 61–101.

Bohacs, K.M., Lazar, O.R., Demko, T.M., 2014. Parasequence types in shelfal mudstone strata—quantitative observations of lithofacies and stacking patterns, and conceptual link to modern depositional regimes. Geology 42 (2), 131–134.

Bonjour, J.L., Dabard, M.P., 1991. Ti/Nb ratios of clastic terrigenous sediments used as an indicator of provenance. Chem. Geol. 91 (3), 257–267.

Borcovsky, D., Egenhoff, S., Fishman, N., Maletz, J., Boehlke, A., Lowers, H., 2017. Sedimentology, facies architecture, and sequence stratigraphy of a Mississippian black mudstone succession—the upper member of the Bakken Formation, North Dakota, United States. Am. Assoc. Pet. Geol. Bull. 101 (10), 1625–1673.

Brown Jr., L.F., Fisher, W.L., 1977. Seismic stratigraphic interpretation of depositional systems: examples from Brazilian rift and pull apart basins. In: Payton, C.E. (Ed.), Seismic Stratigraphy—Applications to Hydrocarbon Exploration: American Association of Petroleum Geologists Memoir. 26. pp. 213–248.

Brumsack, H.J., 2006. The trace metal content of recent organic carbon-rich sediments: implications for Cretaceous black shale formation. Palaeogeogr. Palaeoclimatol. Palaeoecol. 232, 344–361.

Buckman, J., Mahoney, C., März, C., Wagner, T., Blanco, V., 2017. Identifying biogenic silica: mudrock micro-fabric explored through charge contrast imaging. Am. Mineral. 102 (4), 833–844.

Calvert, S.E., Pedersen, T.F., 1993. Geochemistry of recent oxic and anoxic marine sediments: implications for the geological record. Mar. Geol. 113 (1–2), 67–88.

Canfield, D.E., Thamdrup, B., 2009. Towards a consistent classification scheme for geochemical environments, or, why we wish the term 'suboxic'would go away. Geobiology 7 (4), 385–392.

Catuneanu, O., 2002. Sequence stratigraphy of clastic systems: concepts, merits, and pitfalls. J. Afr. Earth Sci. 35, 1–43.

Catuneanu, O., 2006. Principles of Sequence Stratigraphy. Elsevier, Amsterdam.

Catuneanu, O., 2019a. Model-independent sequence stratigraphy. Earth Sci. Rev. 188, 312–388.

Catuneanu, O., 2019b. Scale in sequence stratigraphy. Mar. Pet. Geol. 106, 128–159.

Catuneanu, O., Abreu, V., Bhattacharya, J.P., Blum, M.D., Dalrymple, R.W., Eriksson, P.G., Fielding, C.R., Fisher, W.L., Galloway, W.E., Gibling, M.R., Giles, K.A., Holbrook, J.M., Jordan, R., Kendall, C.G.S., Macurda, B., Martinsen, O.J., Miall, A.D., Neal, J.E., Nummedal, D., Pomar, L., Posamentier, H.W., Pratt, B.R., Sarg, J.F., Shanley, K.W., Steel, R.J., Strasser, A., Tucker, M.E., Winker, C., 2009. Towards the standardization of sequence stratigraphy. Earth Sci. Rev. 92, 1–33.

Catuneanu, O., Galloway, W.E., Kendall, C.G.S., Miall, A.D., Posamentier, H.W., Strasser, A., Tucker, M.E., 2011. Sequence stratigraphy: methodology and nomenclature. Newsl. Stratigr. 44, 173–245.

Chen, H.-F., Yeh, P.-Y., Song, S.-R., Hsu, S.-C., Yang, T.-N., Wang, Y., Chi, Z., Lee, T.-Q., Chen, M.-T., Cheng, C.-L., Zou, J., Chang, Y.-P., 2013. The Ti/Al molar ratio as a new proxy for tracing sediment transportation processes and its application in aeolian events and sea level change in East Asia. J. Asian Earth Sci. 73, 31–38.

Colodner, D., Sachs, J., Ravizza, G., Turekian, K., Edmond, J., Boyle, E., 1993. The geochemical cycle of rhenium: a reconnaissance. Earth Planet. Sci. Lett. 117 (1-2), 205–221.

Crusius, J., Calvert, S., Pedersen, T., Sage, D., 1996. Rhenium and molybdenum enrichments in sediments as indicators of oxic, suboxic and sulfidic conditions of deposition. Earth Planet. Sci. Lett. 145 (1-4), 65–78.

Dashtgard, S.E., MacEachern, J.A., 2016. Unburrowed mudstones may record only slightly lowered oxygen conditions in warm, shallow basins. Geology 44 (5), 371–374.

Davis, C., Pratt, L., Sliter, W., Mompart, L., Mural, B., 1999. Factors influencing organic carbon and trace metal accumulation in the Upper Cretaceous La Luna Formation of the western Maracaibo Basin, Venezuela. In: Barrera, E., Johnson, C.C. (Eds.), Evolution of the Cretaceous Ocean-Climate System, Boulder, Colorado, Geological Society of America Special Paper 332.

Dean, W.E., Arthur, M.A., 1998. Geochemical expressions of cyclicity in Cretaceous pelagic limestone sequences: Niobrara Formation, Western Interior Seaway. In: Dean, W.E., Arthur, M.A. (Eds.), Stratigraphy of Paleoenvironments of the Cretaceous Western Interior Seaway, USA, SEPM Concepts in Sedimentology and Paleontology No. 6. SEPM, Tulsa, OK, United States, pp. 227–255.

DeReuil, A.A., Birgenheier, L.P., 2019. Sediment dispersal and organic carbon preservation in a dynamic mudstone-dominated system, Juana Lopez Member, Mancos Shale. Sedimentology 66 (3), 1002–1041.

Dinelli, E., Tateo, F., Summa, V., 2007. Geochemical and mineralogical proxies for grain size in mudstones and siltstones from the Pleistocene and Holocene of the Po River alluvial plain, Italy. Geol. Soc. Am. Spec. Pap. 420, 25–36.

Dominguez, R.F., Catuneanu, O., 2017. Regional stratigraphic framework of the Vaca Muerta – Quintuco system in the Neuquén Embayment, Argentina. In: Proceedings from: The 20th Geological Congress of Argentina, Tucuman, Argentina.

Dominguez, R.F., Continanzia, M.J., Mykietiuk, K., Ponce, C., Pérez, G., Guerello, R., Lanusse, N.I., Caneva, M., Di Benedetto, M., Catuneanu, O., Cristallini, E., 2016. Organic-rich stratigraphic units in the Vaca Muerta Formation, and their distribution and characterization in the Neuquén Basin (Argentina). In: Proceedings from: Unconventional Resources Technology Conference, San Antonio, Texas.

Egenhoff, S.O., Fishman, N.S., 2013. Traces in the dark—Sedimentary processes and facies gradients in the upper shale member of the Upper Devonian–Lower Mississippian Bakken Formation, Williston Basin, North Dakota, USA. J. Sediment. Res. 83 (9), 803–824.

El Attar, A., Pranter, M.J., 2016. Regional stratigraphy, elemental chemostratigraphy, and

organic richness of the Niobrara Member of the Mancos Shale, Piceance Basin, Colorado. Am. Assoc. Pet. Geol. Bull. 100 (3), 345–377.
Elder, W.P., Gustason, E.R., Sageman, B.B., 1994. Correlation of basinal carbonate cycles to nearshore parasequences in the Late Cretaceous Greenhorn seaway, Western Interior USA. Geol. Soc. Am. Bull. 106 (7), 892–902.
Embry, A.F., 2002. Transgressive-regressive (TR) sequence stratigraphy. In: Proceedings from: 22nd Annual Gulf Coast Section SEPM Foundation Bob F. Perkins Research Conference, Houston, Texas.
Embry, A.F., 2009. Practical sequence stratigraphy. Can. Soc. Petrol. Geol. Reserv. 36, 1–6.
Embry, A.F., 2010. Correlation siliciclastic successions with sequence stratigraphy. In: Ratcliffe, K.T., Zaitlin, B.A. (Eds.), Application of Modern Stratigraphic Techniques: Theory and Case Histories, pp. 35–53 SEPM (Society for Sedimentary Geology) Special Publication, no. 94.
Embry, A.F., Johannessen, E.P., 1993. T–R sequence stratigraphy, facies analysis and reservoir distribution in the uppermost Triassic–Lower Jurassic succession, Western Sverdrup Basin, Arctic Canada. Norw. Petrol. Soc. Spec. Publ. 2, 121–146.
Erickson, B.E., Helz, G.R., 2000. Molybdenum (VI) speciation in sulfidic waters: stability and lability of thiomolybdates. Geochim. Cosmochim. Acta 64 (7), 1149–1158.
Frébourg, G., Ruppel, S.C., Rowe, H., 2013. Sedimentology of the Haynesville (Upper Kimmeridgian) and Bossier (Tithonian) Formations, in the Western Haynesville Basin, Texas, U.S.A. In: Hammes, U., Gale, J. (Eds.), Geology of the Haynesville Gas Shale in East Texas and West Louisiana, U.S.A. pp. 47–67 America Association of Petroleum Geologists Memoir 105.
Froelich, P., Klinkhammer, G.P., Bender, M.L., Luedtke, N.A., Heath, G.R., Cullen, D., Dauphin, P., Hammond, D., Hartman, B., Maynard, V., 1979. Early oxidation of organic matter in pelagic sediments of the eastern equatorial Atlantic: suboxic diagenesis. Geochim. Cosmochim. Acta 43 (7), 1075–1090.
Fru, E.C., Rodríguez, N.P., Partin, C.A., Lalonde, S.V., Andersson, P., Weiss, D.J., El Albani, A., Rodushkin, I., Konhauser, K.O., 2016. Cu isotopes in marine black shales record the Great Oxidation Event. Proc. Natl. Acad. Sci. 113 (18), 4941–4946.
Galloway, W.E., 1989. Genetic stratigraphic sequences in basin analysis I: architecture and genesis of flooding-surface bounded depositional units. Am. Assoc. Pet. Geol. Bull. 73 (2), 125–142.
Gambacorta, G., Trincianti, E., Torricelli, S., 2016. Anoxia controlled by relative sea-level changes: an example from the Mississippian Barnett Shale Formation. Palaeogeogr. Palaeoclimatol. Palaeoecol. 459, 306–320.
Grosjean, E., Adam, P., Connan, J., Albrecht, P., 2004. Effects of weathering on nickel and vanadyl porphyrins of a Lower Toarcian shale of the Paris basin. Geochim. Cosmochim. Acta 68 (4), 789–804.
Gutierrez Parades, H.C., Catuneanu, O., Romano, U.H., 2017. Sequence stratigraphy of the Miocene section, southern Gulf of Mexico. Mar. Pet. Geol. 86, 711–732.
Hammes, U., Frébourg, G., 2012. Haynesville and Bossier mudrocks: a facies and sequence stratigraphic investigation, East Texas and Louisiana, USA. Mar. Pet. Geol. 31 (1), 8–26.
Hammes, U., Hamlin, H.S., Ewing, T.E., 2011. Geologic analysis of the Upper Jurassic Haynesville Shale in east Texas and west Louisiana. Am. Assoc. Pet. Geol. Bull. 95 (10), 1643–1666.
Harazim, D., McIlroy, D., Edwards, N.P., Wogelius, R.A., Manning, P.L., Poduska, K.M., Layne, G.D., Sokaras, D., Alonso-Mori, R., Bergmann, U., 2015. Bioturbating animals control the mobility of redox-sensitive trace elements in organic-rich mudstone. Geology 43 (11), 1007–1010.
Harris, N.B., Mnich, C.A., Selby, D., Korn, D., 2013. Minor and trace element and Re–Os chemistry of the Upper Devonian Woodford Shale, Permian Basin, west Texas: insights into metal abundance and basin processes. Chem. Geol. 356, 76–93.
Harris, N.B., McMillan, J.M., Knapp, L.J., Mastalerz, M., 2018. Organic matter accumulation in the Upper Devonian Duvernay Formation, Western Canada Sedimentary Basin, from sequence stratigraphic analysis and geochemical proxies. Sediment. Geol. 376, 185–203.
Hart, B.S., 2015. The Greenhorn Cyclothem of the Cretaceous Western Interior Seaway: lithology trends, stacking patterns, log signatures, and, and application to the Eagle Ford of West Texas. Gulf Coast Assoc. Geol. Soc. Trans. 65, 155–174.
Helland-Hansen, W., Martinsen, O.J., 1996. Shoreline trajectories and sequences: description of variable depositional-dip scenarios. J. Sediment. Res. 66 (4), 670–688.
Helly, J.J., Levin, L.A., 2004. Global distribution of naturally occurring marine hypoxia on continental margins. Deep-Sea Res. I Oceanogr. Res. Pap. 51 (9), 1159–1168.
Helz, G.R., Miller, C.V., Charnock, J.M., Mosselmans, J.F.W., Pattrick, R.A.D., Garner, C.D., Vaughan, D.J., 1996. Mechanism of molybdenum removal from the sea and its concentration in black shales: EXAFS evidence. Geochim. Cosmochim. Acta 60 (19), 3631–3642.
Hines, B.R., Gazley, M.F., Collins, K.S., Bland, K.J., Crampton, J.S., Ventura, G.T., 2019. Chemostratigraphic resolution of widespread reducing conditions in the southwest Pacific Ocean during the Late Paleocene. Chem. Geol. 504, 236–252.
Huerta-Diaz, M.A., Morse, J.W., 1992. Pyritization of trace metals in anoxic marine sediments. Geochim. Cosmochim. Acta 56 (7), 2681–2702.
Hunt, D., Tucker, M.E., 1992. Stranded parasequences and the forced regressive wedge systems tract: deposition during base-level fall. Sediment. Geol. 81 (1–2), 1–9.
Jaffe, L.A., Peucker-Ehrenbrink, B., Petsch, S.T., 2002. Mobility of rhenium, platinum group elements and organic carbon during black shale weathering. Earth Planet. Sci. Lett. 198 (3–4), 339–353.
Kendall, B., Reinhard, C.T., Lyons, T.W., Kaufman, A.J., Poulton, S.W., Anbar, A.D., 2010. Pervasive oxygenation along late Archaean ocean margins. Nat. Geosci. 3 (9), 647.
Kimura, H., Watanabe, Y., 2001. Oceanic anoxia at the Precambrian-Cambrian boundary. Geology 29 (11), 995–998.
Klinkhammer, G.P., Palmer, M.R., 1991. Uranium in the oceans: where it goes and why. Geochim. Cosmochim. Acta 55 (7), 1799–1806.
Knapp, L.J., McMillan, J.M., Harris, N.B., 2017. A depositional model for organic-rich Duvernay Formation mudstones. Sediment. Geol. 347, 160–182.
Knapp, L.J., Harris, N.B., McMillan, J.M., 2019. A sequence stratigraphic model for the organic-rich Upper Devonian Duvernay Formation, Alberta, Canada. Sediment. Geol. 387, 152–181.
Konhauser, K.O., 2007. Introduction to Geomicrobiology. Blackwell, Malden, Massachusetts.
Lazar, O.R., Bohacs, K.M., Macquaker, J.H., Schieber, J., Demko, T.M., 2015. Capturing key attributes of fine-grained sedimentary rocks in outcrops, cores, and thin sections: nomenclature and description guidelines. J. Sediment. Res. 85 (3), 230–246.
Lemiere, B., 2018. A review of pXRF (field portable X-ray fluorescence) applications for applied geochemistry. J. Geochem. Explor. 188, 350–363.
Lewan, M.D., 1984. Factors controlling the proportionality of vanadium to nickel in crude oils. Geochim. Cosmochim. Acta 48 (11), 2231–2238.
Lewan, M.D., Maynard, J.B., 1982. Factors controlling enrichment of vanadium and nickel in the bitumen of organic sedimentary rocks. Geochim. Cosmochim. Acta 46 (12), 2547–2560.
Li, Z., Schieber, J., 2020. Application of sequence stratigraphic concepts to the Upper Cretaceous Tununk Shale Member of the Mancos Shale Formation, south-central Utah: parasequence styles in shelfal mudstone strata. Sedimentology 67 (1), 118–151.
Liu, Y., Zhang, J., Tang, X., Yang, C., Tang, S., 2016. Weathering characteristics of the Lower Paleozoic black shale in northwestern Guizhou Province, south China. J. Earth Syst. Sci. 125 (5), 1061–1078.
Loutit, T.S., Hardenbol, J., Vail, P.R., Baum, G.R., 1988. Condensed sections: the key to age determination and correlation of continental margin sequences. In: Wilgus, C.K., Hastings, B.S., Kendall, C.G.S., Posamentier, H.W., Ross, C.A., Van Wagoner, J.C. (Eds.), Sea Level Changes – An Integrated Approach: Society of Economic Paleontologists and Geologists Special Publication. 42. pp. 183–213.
MacEachern, J.A., Bann, K.L., Pemberton, S.G., Gingras, M.K., 2009a. The ichnofacies paradigm: high-resolution paleoenvironmental interpretation of the rock record. SEPM Soc. Sediment. Geol. App. Ichnol. SC52, 27–64.
MacEachern, J.A., Pemberton, S.G., Bann, K.L., Gingras, M.K., 2009b. Departures from the archetypal ichnofacies: effective recognition of physico-chemical stresses in the rock record. Soc. Sediment. Geol. Appl. Ichnol. SC52, 65–93.
Macquaker, J.H., Taylor, K.G., 1996. A sequence stratigraphic interpretation of a mudstone-dominated succession: the Lower Jurassic Cleveland ironstone Formation, U.K. J. Geol. Soc. Lond. 153, 759–770.
Macquaker, J.H., Taylor, K.G., Gawthorpe, R.L., 2007. High-resolution facies analyses of mudstones: implications for paleoenvironmental and sequence stratigraphic interpretations of offshore ancient mud-dominated successions. J. Sediment. Res. 77 (4), 324–339.
Mann, U., Stein, R., 1997. Organic facies variations, source rock potential, and sea level changes in Cretaceous black shales of the Quebrada Ocal, Upper Magdalena Valley, Colombia. Am. Assoc. Pet. Geol. Bull. 81 (4), 556–576.
Marynowski, L., Pisarzowska, A., Derkowski, A., Rakociński, M., Szaniawski, R., Środoń, J., Cohen, A.S., 2017. Influence of palaeoweathering on trace metal concentrations and environmental proxies in black shales. Palaeogeogr. Palaeoclimatol. Palaeoecol. 472, 177–191.
McLennan, S.M., Hemming, S., McDaniel, D.K., Hanson, G.N., 1993. Geochemical approaches to sedimentation, provenance, and tectonics. Geol. Soc. Am. Spec. Pap. 284, 21–40.
McManus, J., Berelson, W.M., Klinkhammer, G.P., Hammond, D.E., Holm, C., 2005. Authigenic uranium: relationship to oxygen penetration depth and organic carbon rain. Geochim. Cosmochim. Acta 69 (1), 95–108.
Mongelli, G., Critelli, S., Perri, F., Sonnino, M., Perrone, V., 2006. Sedimentary recycling, provenance and paleoweathering from chemistry and mineralogy of Mesozoic continental redbed mudrocks, Peloritani Mountains, southern Italy. Geochem. J. 40 (20), 197–209.
Morford, J.L., Russell, A.D., Emerson, S., 2001. Trace metal evidence for changes in the redox environment associated with the transition from terrigenous clay to diatomaceous sediment, Saanich Inlet, BC. Mar. Geol. 174 (1–4), 355–369.
Morrison, J.M., Codispoti, L.A., Smith, S.L., Wishner, K., Flagg, C., Gardner, W.D., Gaurin, S., Naqvi, S.W.A., Manghnani, V., Prosperie, L., Gundersen, J.S., 1999. The oxygen minimum zone in the Arabian Sea during 1995. Deep-Sea Res. II Top. Stud. Oceanogr. 46 (8–9), 1903–1931.
Myers, K.J., Wignall, P.B., 1987. Understanding Jurassic organic-rich mudrocks—new concepts using gamma-ray spectrometry and palaeoecology: examples from the Kimmeridge Clay of Dorset and the Jet Rock of Yorkshire. In: Legget, J.K., Zuffa, G.G. (Eds.), Marine Clastic Sedimentology. Springer, Dordrecht, pp. 172–189.
Nadeau, P.H., Wilson, M.J., McHardy, W.J., Tait, J.M., 1985. The conversion of smectite to illite during diagenesis: evidence from some illitic clays from bentonites and sandstones. Mineral. Mag. 49 (352), 393–400.
Nesbitt, H.W., Young, G.M., 1982. Early Proterozoic climates and plate motions inferred from major element chemistry of lutites. Nature 299 (5885), 715–717.
Nyhuis, C.J., Riley, D., Kalasinska, A., 2016. Thin section petrography and chemostratigraphy: integrated evaluation of an upper Mississippian mudstone dominated succession from the southern Netherlands. Neth. J. Geosci. 95 (1), 3–22.
Over, D.J., 1990. Trace metals in burrow walls and sediments, Georgia Bight, USA. Ichnos. Int. J. Plant Anim. 1 (1), 31–41.
Partin, C.A., Bekker, A., Planavsky, N.J., Scott, C.T., Gill, B.C., Li, C., Podkovyrov, V., Maslov, V., Konhauser, K.O., Lalonde, S.V., Love, G.D., Love, G.D., Poulton, S.W., Lyons, T.W., 2013. Large-scale fluctuations in Precambrian atmospheric and oceanic oxygen levels from the record of U in shales. Earth Planet. Sci. Lett. 369, 284–293.
Patchett, P.J., White, W.M., Feldmann, H., Kielinczuk, S., Hofmann, A.W., 1984. Hafnium/rare earth element fractionation in the sedimentary system and crustal recycling into the Earth's mantle. Earth Planet. Sci. Lett. 69 (2), 365–378.

Pearce, T.J., Besly, B.M., Wray, D.S., Wright, D.K., 1999. Chemostratigraphy: a method to improve interwell correlation in barren sequences—a case study using onshore Duckmantian/Stephanian sequences (West Midlands, UK). Sediment. Geol. 124 (1–4), 197–220.
Pearce, T.J., Wray, D., Ratcliffe, K., Wright, D.K., Moscariello, A., 2005. Chemostratigraphy of the Upper Carboniferous Schooner Formation, southern North Sea. In: Collinson, J.D., Evans, D.J., Holliday, D.W. (Eds.), Carboniferous Hydrocarbon Resources: The Southern North Sea and Surrounding Onshore Areas: Occasional Publication Series of the Yorkshire Geological Society. 7. pp. 147–164.
Pearce, T.J., Martin, J.H., Cooper, D., Wray, D.S., 2010. Chemostratigraphy of upper carboniferous (Pennsylvanian) sequences from the Southern North Sea (United Kingdom). In: Application of Modern Stratigraphic Techniques: Theory and Case Histories: SEPM (Society for Sedimentary Geology) Special Publication, 94, pp. 109–127.
Peucker-Ehrenbrink, B., Hannigan, R.E., 2000. Effects of black shale weathering on the mobility of rhenium and platinum group elements. Geology 28 (5), 475–478.
Piper, D.Z., Calvert, S.E., 2009. A marine biogeochemical perspective on black shale deposition. Earth Sci. Rev. 95 (1–2), 63–96.
Plank, T., Langmuir, C.H., 1998. The chemical composition of subducting sediment and its consequences for the crust and mantle. Chem. Geol. 145 (3), 325–394.
Playter, T., Corlett, H., Konhauser, K., Robbins, L., Rohais, S., Crombez, V., Maccormack, K., Rokosh, D., Prenoslo, D., Furlong, C.M., Pawlowicz, J., Gingras, M., Lalonde, S., Lyster, S., Zonneveld, J.-P., 2018. Clinoform identification and correlation in fine--grained sediments: a case study using the Triassic Montney Formation. Sedimentology 65 (1), 263–302.
Plint, A.G., Nummedal, D., 2000. The falling stage systems tract: recognition and importance in sequence stratigraphic analysis. Geol. Soc. Lond., Spec. Publ. 172 (1), 1–17.
Posamentier, H.W., Allen, G.P., 1999. Siliciclastic sequence stratigraphy: concepts and applications. SEPM Soc. Sediment. Geol. Concepts Sedimentol. Paleontol. 7, 210.
Posamentier, H.W., Kolla, V., 2003. Seismic geomorphology and stratigraphy of depositional elements in deep-water settings. J. Sediment. Res. 73 (3), 367–388.
Pyle, L.J., Gal, L.P., 2016. Reference Section for the Horn River Group and Definition of the Bell Creek Member, Hare Indian Formation in central Northwest Territories. Bull. Can. Petrol. Geol. 64 (1), 67–98.
Ratcliffe, K.T., Wright, A.M., Hallsworth, C., Morton, A., Zaitlin, B.A., Potocki, D., Wray, D., 2004. An example of alternative correlation techniques in a low-accommodation setting, nonmarine hydrocarbon system: the (Lower Cretaceous) Mannville Basal Quartz succession of southern Alberta. Am. Assoc. Pet. Geol. Bull. 88 (10), 1419–1432.
Ratcliffe, K.T., Martin, J., Pearce, T.J., Hughes, A.D., Lawton, D.E., Wray, D.S., Bessa, F., 2006. A regional chemostratigraphically-defined correlation framework for the late Triassic TAG-I Formation in Blocks 402 and 405a, Algeria. Pet. Geosci. 12 (1), 3–12.
Ratcliffe, K., Wright, M., Montgomery, P., Palfrey, A., Vonk, A., Vermeulen, J., Barrett, M., 2010. Application of chemostratigraphy to the Mungaroo Formation, the Gorgon field, offshore northwest Australia. APPEA J. 50 (1), 371–388.
Ratcliffe, K.T., Wright, A.M., Schmidt, K., 2012a. Application of inorganic whole-rock geochemistry to shale resource plays: an example from the Eagle Ford Shale Formation, Texas. Sediment. Rec. 10 (2), 4–9.
Ratcliffe, K.T., Woods, J., Rice, C., 2012b. Determining well-bore pathways during multilateral drilling campaigns in shale resource plays: an example using chemostratigraphy from the Horn River Formation, British Columbia, Canada. In: Proceedings from: Eastern Australasian Basin Symposium IV, Brisbane, Australia.
Ratcliffe, K.T., Wright, A.M., Spain, D.R., 2012 April/Mayc. Unconventional methods for unconventional plays: using elemental data to understand shale resource plays. Petrol. Explor. Soc. Aust. News Resour. 117, 50–54.
Reichart, G.J., Lourens, L.J., Zachariasse, W.J., 1998. Temporal variability in the northern Arabian Sea Oxygen Minimum Zone (OMZ) during the last 225,000 years. Paleoceanography 13 (6), 607–621.
Reinhard, C.T., Planavsky, N.J., Robbins, L.J., Partin, C.A., Gill, B.C., Lalonde, S.V., Bekker, A., Konhauser, K.O., Lyons, T.W., 2013. Proterozoic ocean redox and biogeochemical stasis. Proc. Natl. Acad. Sci. 110 (14), 5357–5362.
Revsbech, N.P., Larsen, L.H., Gundersen, J., Dalsgaard, T., Ulloa, O., Thamdrup, B., 2009. Determination of ultra-low oxygen concentrations in oxygen minimum zones by the STOX sensor. Limnol. Oceanogr. Methods 7, 371–381.
Robbins, L.J., Lalonde, S.V., Planavsky, N.J., Partin, C.A., Reinhard, C.T., Kendall, B., Scott, C., Hardisty, D.S., Gill, B.C., Alessi, D.S., Dupont, C.L., Saito, M.A., Crowe, S.A., Poulton, S.W., Bekker, A., Lyons, T.W., Konhauser, K.O., 2016. Trace elements at the intersection of marine biological and geochemical evolution. Earth Sci. Rev. 163, 323–348.
Rosenthal, Y., Lam, P., Boyle, E.A., Thomson, J., 1995. Authigenic cadmium enrichments in suboxic sediments: precipitation and postdepositional mobility. Earth Planet. Sci. Lett. 132 (1–4), 99–111.
Ross, D.J., Bustin, R.M., 2009. Investigating the use of sedimentary geochemical proxies for paleoenvironment interpretation of thermally mature organic-rich strata: examples from the Devonian–Mississippian shales, Western Canadian Sedimentary Basin. Chem. Geol. 260 (1–2), 1–19.
Rowe, H., Hughes, N., Robinson, K., 2012. The quantification and application of handheld energy-dispersive x-ray fluorescence (ED-XRF) in mudrock chemostratigraphy and geochemistry. Chem. Geol. 324–325, 122–131.
Rowe, H.D., Loucks, R.G., Ruppel, S.C., Rimmer, S.M., 2008. Mississippian Barnett Formation, Fort Worth Basin, Texas: bulk geochemical inferences and Mo–TOC constraints on the severity of hydrographic restriction. Chem. Geol. 257 (1–2), 16–25.
Rowe, H., Ruppel, S., Rimmer, S., Loucks, R., 2009. Core-based chemostratigraphy of the Barnett Shale, Permian Basin, Texas. Gulf Coast Assoc. Geol. Soc. Trans. 59, 675–686.
Rowe, H., Wang, X., Fan, B., Zhang, T., Ruppel, S.C., Milliken, K.L., Loucks, R., Shen, Y., Zhang, J., Liang, Q., Sivil, E., 2017. Chemostratigraphic insights into fluvio-lacustrine deposition, Yanchang Formation, Upper Triassic, Ordos Basin, China. Interpretation 5 (2), SF149–SF165.
Sageman, B.B., Lyons, T.W., 2004. Geochemistry of fine-grained sediments and sedimentary rocks. In: Mackenzie, F.T. (Ed.), Sediments, Diagenesis, and Sedimentary Rocks: Treatise on Geochemistry, Second Edition, Volume 7. Elsevier Pergamon, Oxford, United Kingdom, pp. 116–148.
Sano, J.L., Ratcliffe, K.T., Spain, D.R., 2013. Chemostratigraphy of the Haynesville Shale. In: Hammes, U., Gales, J. (Eds.), Geology of the Hanyesville Gas Shale in East Texas and West Louisiana, U.S.A. pp. 137–154 American Association of Petroleum Geologists Memoir 105.
Savrda, C.E., Bottjer, D.J., 1989. Trace-fossil model for reconstructing oxygenation histories of ancient marine bottom waters: application to Upper Cretaceous Niobrara Formation, Colorado. Palaeogeogr. Palaeoclimatol. Palaeoecol. 74 (1–2), 49–74.
Schieber, J., 1994. Evidence for high-energy events and shallow-water deposition in the Chattanooga Shale, Devonian, central Tennessee, USA. Sediment. Geol. 93 (3-4), 193–208.
Schieber, J., 1996. Early diagenetic silica deposition in algal cysts and spores; a source of sand in black shales? J. Sediment. Res. 66 (1), 175–183.
Schieber, J., 1998. Developing a sequence stratigraphic framework for the Late Devonian Chattanooga Shale of the southeastern USA: relevance for the Bakken Shale. In: Christopher, J.E., Gilboy, C.F., Paterson, D.F., Bends, S.L. (Eds.), Eighth International Williston Basin Symposium, pp. 58–68 Saskatchewan Geological Society Special Publication No. 13.
Schieber, J., Krinsley, D., Riciputi, L., 2000. Diagenetic origin of quartz silt in mudstones and implications for silica cycling. Nature 406 (6799), 981.
Schönfeld, J., Kuhnt, W., Erdem, Z., Flögel, S., Glock, N., Aquit, M., Frank, M., Holbourn, A., 2015. Records of past mid-depth ventilation: Cretaceous ocean anoxic event 2 vs. Recent oxygen minimum zones. Biogeosciences 12 (4), 1169–1189.
Scott, C., Lyons, T.W., 2012. Contrasting molybdenum cycling and isotopic properties in euxinic versus non-euxinic sediments and sedimentary rocks: refining the paleoproxies. Chem. Geol. 324–325, 19–27.
Shanmugam, G., 1988. Origin, recognition, and importance of erosional unconformities in sedimentary basins. In: New Perspectives in Basin Analysis. Springer, New York, NY, pp. 83–108.
Shen, J., Zhou, L., Feng, Q., Zhang, M., Lei, Y., Zhang, N., Yu, J., Gu, S., 2014. Paleoproductivity evolution across the Permian-Triassic boundary and quantitative calculation of primary productivity of black rock series from the Dalong Formation, South China. Sci. China Earth Sci. 57 (7), 1583–1594.
Slatt, R.M., Rodriguez, N.D., 2012. Comparative sequence stratigraphy and organic geochemistry of gas shales: Commonality or coincidence? J. Nat. Gas Sci. Eng. 8, 68–84.
Smith, L.B., Schieber, J., Wilson, R.D., 2019. Shallow-water onlap model for the deposition of Devonian black shales in New York, USA. Geology 47 (3), 279–283.
Swift, D.J., 1975. Barrier-island genesis: evidence from the central Atlantic shelf, eastern USA. Sediment. Geol. 14 (1), 1–43.
Taylor, K.G., Macquaker, J.H.S., 2014. Diagenetic alterations in a silt-and clay-rich mudstone succession: an example from the Upper Cretaceous Mancos Shale of Utah, USA. Clay Miner. 49 (2), 213–227.
Taylor, S.R., McLennan, S.M., 1985. The Continental Crust: Its Composition and Evolution. Blackwell, Malden, Massachusetts.
Thomson, J., Higgs, N.C., Croudace, I.W., Colley, S., Hydes, D.J., 1993. Redox zonation of elements at an oxic/post-oxic boundary in deep-sea sediments. Geochim. Cosmochim. Acta 57 (3), 579–595.
Thomson, J., Higgs, N.C., Wilson, T.R.S., Croudace, I.W., De Lange, G.J., Van Santvoort, P.J.M., 1995. Redistribution and geochemical behaviour of redox-sensitive elements around S1, the most recent eastern Mediterranean sapropel. Geochim. Cosmochim. Acta 59 (17), 3487–3501.
Thomson, J., Jarvis, I., Green, D.R., Green, D., 1998. Oxidation fronts in Madeira Abyssal Plain turbidites: persistence of early diagenetic trace-element enrichments during burial, site 9501. In: Weaver, P.P.E., Schmincke, H.-U., Duffield, W. (Eds.), Proceedings of the Ocean Drilling Program, Scientific Results. Vol. 157. pp. 559–571.
Tribovillard, N., Algeo, T.J., Lyons, T., Riboulleau, A., 2006. Trace metals as paleoredox and paleoproductivity proxies: an update. Chem. Geol. 232 (1–2), 12–32.
Turner, B.W., Slatt, R.M., 2016. Assessing bottom water anoxia within the Late Devonian Woodford Shale in the Arkoma Basin, southern Oklahoma. Mar. Pet. Geol. 78, 536–546.
Turner, B.W., Molinares-Blanco, C.E., Slatt, R.M., 2015. Chemostratigraphic, palynostratigraphic, and sequence stratigraphic analysis of the Woodford Shale, Wyche Farm Quarry, Pontotoc County, Oklahoma. Interpretation 3 (1), SH1–SH9.
Turner, B.W., Tréanton, J.A., Slatt, R.M., 2016. The use of chemostratigraphy to refine ambiguous sequence stratigraphic correlations in marine mudrocks. An example from the Woodford Shale, Oklahoma, USA. J. Geol. Soc. 173, 854–868.
Tyson, R.V., Pearson, T.H., 1991. Modern and ancient continental shelf anoxia: an overview. Geol. Soc. Lond., Spec. Publ. 58 (1), 1–24.
Van der Weijden, C.H., 2002. Pitfalls of normalization of marine geochemical data using a common divisor. Mar. Geol. 184 (3–4), 167–187.
Van Wagoner, J.C., Posamentier, H.W., Mitchum, R.M.J., Vail, P.R., Sarg, J.F., Loutit, T.S., Hardenbol, J., 1988. An overview of the fundamentals of sequence stratigraphy and key definitions. In: Wilgus, C.K., Hastings, B.S., Kendall, C.G.S., Posamentier, H.W., Ross, C.A., Van Wagoner, J.C. (Eds.), Sea Level Changes–An Integrated Approach, pp. 39–45 SEPM (Society for Sedimentary Geology) Special Publication 42.
Ver Straeten, C.A., Brett, C.E., Sageman, B.B., 2011. Mudrock sequence stratigraphy: a multi-proxy (sedimentological, paleobiological and geochemical) approach, Devonian Appalachian Basin. Palaeogeogr. Palaeoclimatol. Palaeoecol. 304 (1–2),

54–73.
Wanty, R.B., Goldhaber, M.B., 1992. Thermodynamics and kinetics of reactions involving vanadium in natural systems: accumulation of vanadium in sedimentary rocks. Geochim. Cosmochim. Acta 56 (4), 1471–1483.
Wedepohl, K.H., 1971. Environmental influences on the chemical composition of shales and clays. Phys. Chem. Earth 8, 307–333.
Wignall, P.B., Twitchett, R.J., 1996. Oceanic anoxia and the end Permian mass extinction. Science 272 (5265), 1155–1158.
Wilde, P., Quinby-Hunt, M.S., Erdtmann, B.D., 1996. The whole-rock cerium anomaly: a potential indicator of eustatic sea-level changes in shales of the anoxic facies. Sediment. Geol. 101 (1–2), 43–53.
Williams, C.J., Hesselbo, S.P., Jenkyns, H.C., Morgans-Bell, H.S., 2001. Quartz silt in mudrocks as a key to sequence stratigraphy (Kimmeridge Clay Formation, Late Jurassic, Wessex Basin, UK). Terra Nova 13, 449–455.
Wilson, R.D., Schieber, J., 2015. Sedimentary facies and depositional environment of the Middle Devonian Geneseo Formation of New York, USA. J. Sediment. Res. 85 (11), 1393–1415.
Wyrtki, K., 1962. The oxygen minima in relation to ocean circulation. Deep-Sea Res. Oceanogr. Abstr. 9 (1-2), 11–23.
Yamashita, Y., Takahashi, Y., Haba, H., Enomoto, S., Shimizu, H., 2007. Comparison of reductive accumulation of Re and Os in seawater–sediment systems. Geochim. Cosmochim. Acta 71 (14), 3458–3475.
Zhang, J., Zeng, Y., Slatt, R., 2019. XRF (X-ray fluorescence) applied to characterization of unconventional Woodford Shale (Devonian, USA) lateral well heterogeneity. Fuel 254, 115565.
Zhou, C., Jiang, S.Y., 2009. Palaeoceanographic redox environments for the lower Cambrian Hetang Formation in South China: evidence from pyrite framboids, redox sensitive trace elements, and sponge biota occurrence. Palaeogeogr. Palaeoclimatol. Palaeoecol. 271 (3–4), 279–286.